A CLIMATOLOGY OF THE ARCTIC ON MID-TROPOSPHERIC TEMPERATURE REGULATION

A Thesis

by

JEREMY PATRICK ANTHONY

Submitted to the Office of Graduate and Professional Studies of
Texas A&M University
in partial fulfillment of the requirements for the degree of

MASTER OF SCIENCE

Chair of Committee,	Robert L. Korty
Committee Members,	Gerald R. North
	Oliver W. Frauenfeld
Head of Department,	Ping Yang

August 2014

Major Subject: Atmospheric Sciences

ABSTRACT

The Arctic is a unique and complex environment. Many factors play a role in determining the long-term climate of the Arctic, including mesoscale weather systems and many complex ice-albedo feedback mechanisms. Previous studies determined using real observations that although 500 hPa temperatures reach $-45\,^{\circ}\mathrm{C}$ by mid-November, temperatures very rarely drop below, despite a total loss of incoming solar radiation. This temperature value at 500 hPa follows moist-adiabatically to the surface value of approximately $-2\,^{\circ}\mathrm{C}$, which is the freezing point of high-latitude sea water.

Sea ice data was examined using satellite and model data to paint a picture of the environment during three distinct periods in history: the last glacial maximum (twenty-one thousand years ago), the mid-Holocene (six-thousand years ago), and the 20th century. Areal September minimum sea ice extent has reached record lows annually since 2007. Vertical temperature profiles created with CCSM4 model data during these three eras show the atmosphere becoming more moist-adiabatic at high latitudes over time. Saturation potential vorticity allows us to assess the convective environment, and it shows that the Arctic is becoming more tropical over time. Analysis of areal extent where temperatures fall below $-45\,^{\circ}\mathrm{C}$ at 500 hPa shows this to be an extremely rare occurrence, and temperatures never fall below $-47.5\,^{\circ}\mathrm{C}$, except for very rare occurrences during the last glacial maximum. Transient eddy heat flux is increasing at higher latitudes, and the warm half of a cyclone contains convection (as seen in saturation potential vorticity). In this paper, we present several lines of evidence supporting a role for intermittent convection in maintaining mid-tropospheric temperatures across climate states of the past twenty-one thousand

years.

DEDICATION

To my family. My little family has always been the inspiration behind my educational goals. When Tyler was born, the first promise I made when I held him was that I would finish my degree, so that I could give him a better life than I had growing up. When he was little, he snuck a few of his crayons into my backpack before my first day at A&M. He just assumed I needed them. I carried those crayons in my pocket when I walked the stage two and a half years later. My wife, Ashley Rae, put her career ambitions on hold because she knew how important this was to me. She picked up her Texas roots and moved cross-country, each time to a place she'd never been, without question. There's no better way to keep your sanity through stressful situations than by surrounding yourself with people you genuinely enjoy spending your time with. We found out about Charlie girl the weekend before grad school started, and she's managed to keep me grounded (and busy) throughout. Sometimes you have bad days. But those never lasted long, because whenever I went home, she'd greet me with a smile and a book - and we'd read and laugh the troubles away.

Finally, thank you to my parents. We never had much growing up, but we always knew the only real way out of poverty was an education. My sister and I both have a college education today, thanks in large part to the backbreaking work my dad endured in order to provide for us. Your work did not go unnoticed, and you will never go unappreciated.

ACKNOWLEDGEMENTS

I would like to thank my committee: Dr. Korty, Dr. North, and Dr. Frauenfeld for their dedication and availability to me on both a personal and professional level. Dr. North has been a mentor to me since my first Thermodynamics course in the spring of 2007. A trip to Dr. North's office was always met with countless stories of things he's encountered along the way, and guidance for my journey. Dr. North is a big reason for my interest in climatology. Similarly, Dr. Frauenfeld's course on Arctic Climates is a big reason for my interest in the Arctic. He encouraged us to challenge peer-reviewed literature, by asking how we could make the studies better. But I am especially thankful for the guidance I received at Texas A&M University from Dr. Korty. His incredible patience and willingness to be involved in all levels of my research has made my second stay at A&M very special.

I worked for Colonel Steven Cahanin at Patrick AFB. Although my career trajectory didn't yet call for advanced education, Col Cahanin believed that I was ready. The Colonel nudged me down the path he followed years ago, and I will spend my Air Force career striving to meet the goals and standards he's established for me. I wish you well in retirement, Colonel, although you could have picked a better state.

TABLE OF CONTENTS

Page

ABSTRACT ii

DEDICATION iv

ACKNOWLEDGEMENTS v

TABLE OF CONTENTS vi

LIST OF FIGURES viii

LIST OF TABLES xi

1. INTRODUCTION 1

2. BACKGROUND 4

3. MODEL INFORMATION 9

3.1 Methods 10

4. ARCTIC CLIMATES 12

4.1 Normalized Sea Ice Concentration 12
4.2 September Sea Ice Area 13
4.3 Arctic Vertical Temperature Profiles 14
4.4 North Atlantic Storm Track 15
4.5 Canadian Arctic Archipelago 16
4.6 Regions with High P* Differences 17

5. MINIMUM MID-TROPOSPHERIC TEMPERATURES 19

5.1 NCEP/NCAR Area 19
5.2 CCSM4 Area 20

6. SATURATION POTENTIAL VORTICITY AND TRANSIENT EDDY FLUX 24

6.1 Saturation PV 24
6.2 Cross-sectional P* 26

6.3 Last Glacial Maximum - 20th Century Differences 28
6.4 Mid-Holocene - 20th Century Differences 29
6.5 NCEP −45 °C Areal Anomalies 30
6.6 Mid-latitude and Arctic Heat Flux 31

7. SUMMARY AND CONCLUSIONS 35

REFERENCES 38

APPENDIX A. FIGURES 42

APPENDIX B. TABLES 93

LIST OF FIGURES

FIGURE Page

A.1 CCSM4 - Last Glacial Maximum September mean sea ice concentration 42

A.2 CCSM4 - Mid-Holocene September mean sea ice concentration 43

A.3 CCSM4 - 20th Century September mean sea ice concentration 44

A.4 NCEP/NCAR - North Pole Skew-T log-P 45

A.5 CCSM4 - Iceland DJF Skew-T log-P 65.5 °N 7.5 °W 46

A.6 CCSM4 - Jan Mayen DJF Skew-T log-P 71.2 °N 7.5 °W 47

A.7 CCSM4 - DJF Skew-T log-P 74.9 °N 7.5 °W 48

A.8 CCSM4 - Canadian Arctic Archipelago DJF Skew-T log-P 65 °N 110 °W 49

A.9 CCSM4 - Canadian Arctic Archipelago DJF Skew-T log-P 71 °N 110 °W 50

A.10 CCSM4 - Canadian Arctic Archipelago DJF Skew-T log-P 75 °N 110 °W 51

A.11 CCSM4 - Canadian Arctic Archipelago DJF Skew-T log-P 80 °N 110 °W 52

A.12 CCSM4 - Canadian Arctic Archipelago DJF Skew-T log-P 85 °N 110 °W 53

A.13 CCSM4 - Mean North Atlantic Storm Track (60 °N-80 °N/0 °E-50 °E) DJF Skew-T log-P 54

A.14 CCSM4 - Mean North American coast (50 °N-60 °N/60 °W-10 °W) DJF Skew-T log-P 55

A.15 NCEP - Satellite era Arctic area where 500 hPa temperatures <-40 °C in km^2 56

A.16 NCEP - Satellite era Arctic area where 500 hPa temperatures <-42.5 °C in km^2 57

A.17 NCEP - Satellite era Arctic area where 500 hPa temperatures <-45 °C in km^2 58

A.18 CCSM4 - 20thc Arctic area where 500 hPa temperatures $<-40\,^{\circ}\mathrm{C}$ in km^2 59

A.19 CCSM4 - 20thc Arctic area where 500 hPa temperatures $<-42.5\,^{\circ}\mathrm{C}$ in km^2 60

A.20 CCSM4 - 20thc Arctic area where 500 hPa temperatures $<-45\,^{\circ}\mathrm{C}$ in km^2 61

A.21 CCSM4 - Last Glacial Maximum Arctic area where 500 hPa temperatures $<-40\,^{\circ}\mathrm{C}$ in km^2 62

A.22 CCSM4 - Last Glacial Maximum Arctic area where 500 hPa temperatures $<-42.5\,^{\circ}\mathrm{C}$ in km^2 63

A.23 CCSM4 - Last Glacial Maximum Arctic area where 500 hPa temperatures $<-45\,^{\circ}\mathrm{C}$ in km^2 64

A.24 CCSM4 - Last Glacial Maximum Arctic area where 500 hPa temperatures $<-47.5\,^{\circ}\mathrm{C}$ in km^2 65

A.25 CCSM4 - Mid-Holocene Arctic area where 500 hPa temperatures $<-40\,^{\circ}\mathrm{C}$ in km^2 66

A.26 CCSM4 - Mid-Holocene Arctic area where 500 hPa temperatures $<-42.5\,^{\circ}\mathrm{C}$ in km^2 67

A.27 CCSM4 - Mid-Holocene Arctic area where 500 hPa temperatures $<-45\,^{\circ}\mathrm{C}$ in km^2 68

A.28 CCSM4 - Moist adiabatic temperature profile where P* 0 over Iceland 69

A.29 CCSM4 - Last glacial maximum P* cross section taken at 60 °N in PVU 70

A.30 CCSM4 - Last glacial maximum P* cross section taken at 65 °N in PVU 71

A.31 CCSM4 - Last glacial maximum P* cross section taken at 70 °N in PVU 72

A.32 CCSM4 - Mid-Holocene P* cross section taken at 60 °N in PVU . . . 73

A.33 CCSM4 - Mid-Holocene P* cross section taken at 65 °N in PVU . . . 74

A.34 CCSM4 - Mid-Holocene P* cross section taken at 70 °N in PVU . . . 75

A.35 CCSM4 - 20th Century maximum P* cross section taken at 60 °N in PVU 76

A.36 CCSM4 - 20th Century P* cross section taken at 65 °N in PVU . . . 77

A.37 CCSM4 - 20th Century P* cross section taken at 70 °N in PVU . . . 78

A.38 CCSM4 - Normalized 775 hPa DJF Last Glacial Maximum-20th Century P* <0.15 in PVU . . . 79

A.39 CCSM4 - Normalized 550 hPa DJF Last Glacial Maximum-20th Century P* <0.15 in PVU . . . 80

A.40 CCSM4 - Normalized 350 hPa DJF Last Glacial Maximum-20th Century P* <0.15 in PVU . . . 81

A.41 CCSM4 - Normalized 775 hPa DJF Mid-Holocene-20th Century P* <0.15 in PVU . . . 82

A.42 CCSM4 - Normalized 550 hPa DJF Mid-Holocene-20th Century P* <0.15 in PVU . . . 83

A.43 CCSM4 - Normalized 350 hPa DJF Mid-Holocene-20th Century P* <0.15 in PVU . . . 84

A.44 NCEP - 775 hPa P* from December 1950, January, and February 1951 in PVU . . . 85

A.45 NCEP - 550 hPa P* from December 1950, January, and February 1951 in PVU . . . 86

A.46 NCEP - 775 hPa P* from January, February, and March 1979 in PVU 87

A.47 NCEP - 550 hPa P* from January, February, and March 1979 in PVU 88

A.48 November through March mean transient eddy heat flux during the last glacial maximum in K*m/s . . . 89

A.49 November through March mean transient eddy heat flux during the mid-Holocene in K*m/s . . . 90

A.50 November through March mean transient eddy heat flux during the 20th century in K*m/s . . . 91

A.51 November through March differential mean transient eddy heat flux between the last glacial maximum and the 20th century (top) and the mid-Holocene and the 20th century (bottom) in K*m/s. Note the difference in scale. . . . 92

LIST OF TABLES

TABLE Page

B.1 Normalized Sea Ice Fraction 93

B.2 Total Transient Eddy Heat Flux (J kg^{-1} m/s) 93

1. INTRODUCTION

The Arctic is a unique and complex environment. Many factors play a role in determining the long-term climate of the Arctic, including mesoscale weather systems and many complex ice-albedo feedback mechanisms. Feedback loops and interactions involving primarily sea ice and snow cover lead to the theory where greenhouse-induced warming effects are expected to be enhanced and accelerated in the Arctic region in comparison with that for the entire globe. Surface temperatures during the Arctic winter are among the coldest in the world. In the winter, ambient temperatures can drop well into the $-70\,^{\circ}\mathrm{C}$ range, making the Arctic home to some of the most bitter conditions on the planet.

The last 21,000 years have seen a notable rise in temperatures throughout the Arctic atmosphere. The rise in Arctic near-surface air temperatures has been almost twice as large as the global average in recent decades due to a process called Arctic amplification (Screen and Simmonds, 2010). Additionally, a compilation of paleoclimate records from lake sediments, trees, glaciers, and marine sediments showed that between 1840 and the mid-20th century, the Arctic warmed to the highest temperatures in four centuries (Overland et al., 1997). As a result, total areal sea ice coverage declined in the 20th century and continues to do so into the 21st. The implications of an ice-free Arctic to the rest of the planet are innumerable.

The 500 hectopascal (hPa) level is the mid-point for all atmospheric mass, and a group discovered a notable difference concerning one specific characteristic at this level in the early 21st century. The group discovered that Arctic 500 hPa temperatures very rarely dropped below $-45\,^{\circ}\mathrm{C}$, despite a continued net radiative loss throughout the winter season (Chase et al., 2002). An idea emerged concerning natural regulation

of mid-tropospheric temperatures. The group postulated that the value itself is significant, because tracing $-45\,^{\circ}\mathrm{C}$ to the surface along a moist adiabat using a skew-T log-p diagram yields a surface value of $-2\,^{\circ}\mathrm{C}$, which is roughly the freezing point of sea water. The implication here is that mid-tropospheric temperatures are controlled by convection from Arctic air masses interacting with open ocean either locally or to the south. Even the smallest opening in the sea ice gives way to convection caused by the interaction of the relatively warmer water with the much colder near-surface air, thus creating a mechanism for the transport of heat from the surface waters to the mid-troposphere.

Convection is important to the thermal stratification within the Arctic itself. The typical Arctic atmospheric profile is stable in most cases, with the presence of a very strong low-level inversion. The zonal mean thermal stratification is only moist adiabatic equatorward of $30\,^{\circ}\mathrm{N}$ in January and equatorward of $50\,^{\circ}\mathrm{N}$ in July, meaning deep moist convection may be important at low latitudes for maintaining vertical thermal stratification (Korty and Schneider, 2007). Poleward of these latitudes, vertical temperature profiles are more stable than moist adiabats in the zonal mean, particularly in the lower troposphere (Schneider, 2004). Examining lapse rates in the Arctic can tell us whether or not higher latitudes are experiencing changes in the physics establishing thermal structure.

Because traditional convection in the Arctic is typically infrequent, using the simple diagnostic tool saturation potential vorticity (P*) will allow us to also examine the possibility of slantwise convection as an alternative. Six-hourly P* data can tell us about the timing and location of convective activity along the storm tracks, as well as areas prone to rapid temperature changes, such as land and exposed ocean surfaces. This tool ultimately gives us a picture of the role convection plays in the process of mid-tropospheric temperature regulation.

Our present goal is to analyze the evolution over time of areal extent of temperatures at the 500 hPa level using the Community Climate System Model 4.0 (CCSM4) from the Community Earth System Model (CESM). Because past works have only analyzed 20th century areal data, this work will serve to enhance the idea postulated by Chase (2002) on a natural mid-tropospheric temperature regulation mechanism. Further, evaluation of P* and heat flux will serve to tell us about the evolution of the mechanism involved in 500 hPa temperature regulation itself. Providing a roadmap for the evolution of heat flux over time will make the picture on how open ocean could be responsible for mid-tropospheric temperature regulation even more clear. Analysis of heat flux data over several distinct periods in time will serve to aid our efforts. Our primary goal is to understand the long-term evolution of such mechanisms and the inherent feedback mechanism moving forward.

2. BACKGROUND

Since Arctic sea ice reached its lowest areal extent in the satellite record in September 2007, measuring 40% below the long-term mean (Comiso et al., 2008), the period from 2007-2012 has witnessed the six lowest September sea ice extents in the modern record (Screen and Simmonds, 2013). The dwindling Arctic ice cover has been cited as a cause of recent changes in Arctic air temperature and humidity (Serreze et al., 2009), storm activity (Simmonds and Keay, 2009) and tropospheric circulation patterns (Francis et al., 2009). Spatial analysis between 1979-2012 shows the total annual sea ice extent in the Arctic declining.

Analyzing pressure trends in the Arctic shows a steady decline in mean pressure values in the region. The degree to which cold air penetrates into middle latitudes is related to the Arctic Oscillation (AO) index, or Northern Annular Mode (NAM), which is determined by surface atmospheric pressure patterns. When the AO index is positive, surface pressure is low in the polar region. This helps the mid-latitude jet stream to blow strongly and consistently from west to east, thus keeping cold Arctic air locked in the polar region. When the AO index is negative, there tends to be high pressure in the polar region, weaker zonal winds, and greater movement of frigid polar air into middle latitudes (Hansen et al., 2010).

Present day Arctic conditions are met with lower mean surface pressure levels and a lower concentration of sea ice. Stieglitz et al. (2003) found through borehole examination that the coasts of Alaska and the Canadian Arctic Archipelago are warming at a faster rate than their inland counterparts. The AO/NAM appears to have strong ties with Arctic sea ice (Serreze and Francis, 2006). As AO/NAM rises toward a positive state, the associated wind field helped to break up winter ice

cover along the Siberian and Alaskan coasts, resulting in thinner ice in spring that is more vulnerable to summer decay (Rigor et al., 2002). Liu et al., (2012) showed that decreasing sea ice concentration by 1% leads to a 0.36%-0.47% increase in cloud cover. Clouds in the Arctic act as a warming mechanism eleven months a year, with July being the only month they act as a cooling mechanism.

Fang and Wallace (1994) showed a strong correlation between 500 hPa heights and sea ice concentration. Francis and Vavrus (2012) analyzed daily fields of 500 hPa heights from NCEP reanalysis over North America to assess changes in north-south Rossby wave characteristics associated with Arctic amplification and the relaxation of poleward thickness gradients. Two effects are identified that each contributes to a slower eastward progression of Rossby waves in the upper-level flow: 1) Weakened zonal winds and 2) increased wave amplitude. Slower progression of upper-level waves causes more persistent weather conditions that can increase the likelihood of certain types of extreme weather, such as drought, prolonged precipitation, cold spells and heat waves at mid-latitudes. Ridge elongation is also expected in response to larger increases in 500 hPa heights at high latitudes than at mid-latitudes. This effectively stretches the peaks of ridges northward and further augments the wave amplitude and higher amplitude waves also tend to progress more slowly, as well as further south over time. Interestingly, Strong and Davis (2007) showed that the circumpolar vortex and the subtropical jet are out of phase with one another, and while a warming Arctic would be expected to slow the jet stream, the opposite is occurring, largely due to the increasing strength of the Hadley circulation.

Chase et al., (2002) found that 500 hPa temperatures in the Arctic fall below $-40\,^{\circ}\mathrm{C}$ by mid November in most years, but rarely fall below this value into the winter months, even though net radiative loss continues. Their work outlines areal extent of 500 hPa temperatures below $-40\,^{\circ}\mathrm{C}$, $-42\,^{\circ}\mathrm{C}$, $-44\,^{\circ}\mathrm{C}$, and $-46\,^{\circ}\mathrm{C}$, finding that

temperatures seldom fall below $-44\,^{\circ}\mathrm{C}$ and never fall below $-46\,^{\circ}\mathrm{C}$ from 1950-1998 using the NCEP/NCAR reanalysis data set. Sea surface salinity of unfrozen waters in the Arctic during the 20th century is roughly 35 practical salinity units (PSU), which sets a freezing temperature of $-1.9\,^{\circ}\mathrm{C}$ for seawater. Taking this value along a moist adiabatic ascent yields a temperature value slightly below $-45\,^{\circ}\mathrm{C}$. The association between 500 hPa levels and sea surface temperatures (SSTs) has been maintained consistently.

One hypothesis is that Arctic air masses dip far enough to the south during winter months to ensure contact with unfrozen open ocean surfaces. The open ocean surface temperatures being not lower than $-1.9\,^{\circ}\mathrm{C}$ react with the much colder air mass to initiate convection. Convective heating provides vertical heat transport that warms the entire column of air rather quickly. The air mass begins to cool immediately upon passing over ice or land masses, but the process is slow, such that mid-tropospheric temperatures remain undisturbed from their relatively warm state for longer periods of time. Further, downward radiation at the surface is a strong function of mid-tropospheric temperatures, which implies the indirect feedback mechanism results in warmer surface temperatures. The group found that all winter months show warming over the last half century at all levels throughout the atmosphere (Chase et al., 2002). The authors of this research have encouraged further research to be conducted using model data reaching into different periods of time (Chase et al., 2002).

In order to more fully investigate what roles convection may play in establishing middle tropospheric winter temperatures in the Arctic, we undertake an analysis of the frequency and climatology of convective activity at high latitudes during winter months. Korty and Schneider (2007) showed that even though mean lapse rates are decidedly stable at middle and high latitudes during winter (see, for example, Stone and Carlson [1979]), convection regularly occurs. They found this especially

occurs over the ocean storm tracks, but even high latitude continents and the Arctic displayed some evidence of convective activity during January.

Tropical and middle latitude summer convection that occurs in isolated cells is upright, where buoyant, unstable parcels displaced vertically rise against the gravitational vector to their level of neutral buoyancy. Unstable buoyant parcels subject to restoring forces of both gravitational and centrifugal accelerations rise along slanted angular momentum paths in a process called symmetric instability (Emanuel 1983). This process is readily observed in the inner core of tropical cyclones, in frontal boundaries of middle latitude cyclones, and near the Arctic polar front (e.g., Emanuel 2008). Although the lateral scale of these convective motions is larger than that for upright convection, both transport heat vertically and establish moist adiabatic lapse rates, albeit symmetric instabilities accomplish this along tilted angular momentum surfaces as opposed to vertical soundings at a fixed station.

In order to capture both mechanisms for convective instability, and in recognition of the fact that symmetric instabilities may occupy a disproportionately large fraction of convective events in high latitude storms (Korty and Schneider 2007; Emanuel 2008), we calculate the saturation potential vorticity (P*). This quantity measures the alignment of gradients of saturation equivalent potential temperature and angular momentum surfaces, as the latter is parallel to the absolute vorticity vector (Frisus 2005) central to the definition of Ertel (1942) potential vorticity (P):

$$P = \frac{(2\mathbf{\Omega} + \nabla \times \mathbf{u}) \cdot \nabla\theta}{\rho} \tag{2.1}$$

In the case of P*, we use saturation equivalent potential temperature (θ_e^*) in place of virtual potential temperature (θ):

$$P^* = \frac{(2\boldsymbol{\Omega} + \nabla \times \mathbf{u}) \cdot \nabla \theta^*_{\mathbf{e}}}{\rho} \tag{2.2}$$

Changes in the Emanuel P* values, specifically the frequency of values approaching or below zero, should reveal whether or not Arctic air is acquiring characteristics more common to lower latitudes, where convection plays some role in establishing the stratification. This will reveal the trend in lapse rates and give us some insight into whether or not the frequency of convection in the Arctic is changing.

Sampling three distinct time periods gives us a look into changes in different climates. Morgan (1945) outlines the timing of perihelion on earth. The last glacial maximum, 21,000 years ago, was a period where much of the earth was covered in ice. Earth was a much colder place, yet the orbital procession was in phase with earth today. The mid-Holocene, 6,000 years ago, is a period where the climate was very similar to earth's climate today, but the orbital procession was out of phase with today's planet. And finally, the 20th century gives us a glimpse at the impact of mechanisms at work on our present environment.

3. MODEL INFORMATION

The Community Climate System Model (CCSM) is a general circulation climate model consisting of atmosphere, land, ocean, and sea ice components that are linked through a coupler that exchanges state information and fluxes between the components.

For this study, we use a collection of models and data sets. Examination of sea ice coverage in the northern hemisphere is accomplished using sea ice data from the National Snow and Ice Data Center (NSIDC). The data is generated from brightness temperature data derived from the following satellite sensors: the Nimbus-7 Scanning Multichannel Microwave Radiometer (SMMR), the Defense Meteorological Satellite Program (DMSP) F8, -F11 and F13 Special Sensor Microwave/Imagers (SSM/Is), and the DMSP-F17 Special Sensor Microwave Imager/Sounder (SSMIS). This data is provided in the polar stereographic projection at a grid cell size of 25 x 25 kilometers. Spatial analysis between 1979-2013 is accomplished (Njoku, 2004).

The National Center for Environmental Prediction/National Center for Atmospheric Research (NCEP/NCAR) Reanalysis model provides data from 1948-present (continuing) for 17 pressure levels at 2.5° resolution. We use 6-hourly and monthly mean reanalysis data to provide a background with which we can verify the findings of similar research in the field (Kalnay et al., 1996).

The Community Climate System Model (CCSM) is a general circulation climate model consisting of atmosphere, land, ocean, and sea ice components that are linked through a coupler that exchanges state information and fluxes between the components. The Community Earth System Model (CESM) is the ongoing project that created the Community Climate System Model version 4.0 (CCSM4), which was

designed to understand and predict the climate system. CCSM4 is a fully-coupled, community, global climate model that provides state-of-the-art computer simulations of the Earth's past, present, and future climate states at a resolution of 1° (Gent, 2011). The CCSM4 data were downloaded directly from the mass storage system at the National Center for Atmospheric Research (NCAR); these files are also available from CMIP5 archives. We use 6-hourly time steps for three distinct periods in our study: 1. Last glacial maximum 2. 20th century 3. Mid-Holocene epoch. The Last Glacial Maximum simulation is an equilibrium simulation forced with conditions present 21,000 years ago. The data is the last 30 years of an equilibrium run. The Mid-Holocene is an equilibrium simulation forced with conditions present 6,000 years ago. The data is the last 30 years of an equilibrium run. The 20th century run uses time-varying forcing for the years of the 20th century, where the years 1971-2005 were used in this study.

3.1 Methods

We consider the Arctic to be the area of earth north of 60 °N. First, we assess changes in sea ice fraction over the three periods of the CCSM4 model run. Because a good portion of the water is locked up in ice over Eurasia and North America during the last glacial maximum time period, the coastlines are different than they are for the other two periods. Thus in order to assess the changes, we normalized this data by taking the total sea ice coverage divided by the total available ocean surface for each time period.

Next, we discuss changes in skew-T log-p vertical temperature profiles by taking specific points in the North Atlantic for each of the three periods. We assess the changes in areal extent of the −45 °C isotherm at the 500 hPa level by assigning a logical identifier to each grid point below the thresholds −40 °C, −42.5 °C, and

−45 °C. Then, we multiply by the area of each specific grid box and sum the areas in the region. This gives us total areal extent of the Arctic below each isotherm. Vertical temperature profiles give us a snapshot of the changing surface temperatures, thereby allowing for Arctic air masses to come into contact with open-ocean surfaces.

Cross-sectional saturation potential vorticity figures are made using six-hourly temperature, zonal and meridional winds from the CCSM4 model run for each period. The figures are plotted along the 60 °N and 70 °N latitude bands and show vertical extent of saturation potential vorticity. Differential plots are shown between the last glacial maximum and 20th century and the mid-Holocene and 20th century. Two cases are assessed using NCEP/NCAR temperature, zonal and meridional winds for saturation potential vorticity calculation. Saturation potential vorticity allows us to quickly diagnose both vertical and slantwise convection, thereby showing the mechanism by which heat is transported aloft.

Transient eddy flux is calculated over the three periods using CCSM4 data, where the total meridional sensible heat flux is a variable provided by the model, as are temperature and meridional winds. The transient eddy flux is calculated as a differential of the total meridional sensible heat flux and the mean flux from this data and plotted at the 500 hPa level. Transient eddy flux shows the heat transported aloft as a result of transient eddies, which are propagated as one result of convection.

The hypothesis is that Arctic air masses dip far enough south to come into contact with open-ocean surfaces, thus providing the mid-troposphere with heat sufficient to regulate minimum mid-tropospheric temperatures. Further, convection is the mechanism driving mid-tropospheric temperatures, so we provide a road map of how convection changes over the time periods. Ensemble data was not used in this study.

4. ARCTIC CLIMATES

Arctic sea ice plays an important role in earth's climate. Ice has an extremely high albedo, which means radiation incident on the surface is almost entirely reflected. A cloud-free Arctic loses such radiation to space, while different periods of the year leave the region insulated with relatively abundant cloud cover. Ice also works to create a natural thermal inversion, as surface temperatures remain lower than the air aloft. The presence of Arctic sea ice also works to maintain a strong horizontal temperature gradient between the equatorial region and the poles, thus regulating polar front jet wind speeds and location in the northern hemisphere. A lack of sea ice in the Arctic region arguably has more of an effect, however. Most snowfall in the region has ceased by the end of May, and as the snow decays, it leaves melt ponds on the surface of the ice. Water has a much lower albedo than ice, thus solar radiation incident on its surface is absorbed rather than reflected (Curry, 1995). This positive feedback loop warms the surface, further melts the ice, which changes the surface albedo and continues the process.

4.1 Normalized Sea Ice Concentration

We looked at sea ice concentration over three eras: the last glacial maximum, mid-Holocene, and the 20th century using CCSM4 model data. When examining sea ice change over time, it is important to first consider the era. The last glacial maximum and 20th century are more straight-forward. Earth's perihelion, where earth is closest to the sun, occurs in January, while the mid-Holocene experienced perihelion in the late summer (Clement et al., 2000). Water has a higher heat capacity than land, thus it takes much longer to heat up and cool down. This results in a lag in the effects of incident solar radiation, and thus one might expect a stronger

northern hemisphere summer in the mid-Holocene to result in a later season sea ice minimum relative to the other two eras.

During the last glacial maximum, ice sheets largely covered North America and Eurasia. Because of this, the oceans were volumetrically smaller, thus the coasts of land masses were extended into areas covered today by water. Thus it is important to normalize the scale we use in order to compare changes over the three eras. CCSM4 provides a land fraction for our region, north of 60 °N. Creating a ratio of ice fraction divided by one minus land fraction is a way of normalizing our data, the results of which are provided in Table B.1.

Analyzing the table shows us first that August and September are the months of minimum sea ice extent for all three eras. While the lag related to absorption of incident solar radiation still exists, the assumption that a later sea ice minimum during the mid-Holocene exists is untrue. Regardless of the timing of earth's perihelion, northern hemisphere summer is the same in all three eras.

4.2 September Sea Ice Area

Three figures will illustrate the differences in sea ice minimum over the three eras and allow us to draw very broad initial conclusions. During the last glacial maximum, sea ice was entirely uniform in the Arctic Sea. Figure A.1 shows the only major area with intermittent breaks was along the North Atlantic storm track, off the east coast of Greenland, northwest along the coast of Scandinavia. An area in the central Baffin Bay off the west coast of Greenland has another concentrated area where the sea ice had intermittent breaks.

The mid-Holocene shows immediate noticeable differences from the last glacial maximum. The ice sheets over North America and Eurasia are gone, and we see in Figure A.2 that the coasts show large sections of surface area where the ratio of

seawater to sea ice is less than 0.5. Entire areas approaching north to the pole are no longer completely covered by the ice sheet, including the North Atlantic storm track.

Figure A.3 shows us that 20th century sea ice extent is most closely related to the mid-Holocene. Still less of the Arctic Ocean is covered completely by solid ice and the fraction of the sea covered by ice is much lower near the continents. The North Atlantic storm track, the Beaufort Sea, and the East Siberian Sea stand out as areas where there are notable breaks in the sea ice.

4.3 Arctic Vertical Temperature Profiles

Arctic vertical temperature profiles are typically very stable. Figure A.4 is an example of a typical Arctic vertical temperature profile: cold air at the surface under relatively warmer air aloft, with a stable profile relative to a moist adiabat up to the tropopause, where the air then follows a dry adiabat. A stable atmosphere means several things for the region. First, convection is infrequent, thus precipitation is limited. The Arctic is considered a desert due to the natural Hadley/Ferrel/Polar cell model circulation, which shows rising air at the equator and 60 ° with sinking air at 30 ° and the poles. Earth's major deserts all reside in or very near those zones of sinking air. A stable atmosphere also means more clear skies, which means more loss of solar radiation to space. Finally, a stable atmosphere means there is nothing happening to break up the extremely highly reflective sea ice surface. This means even more net radiative loss in the region.

Over time, however, mean vertical temperature profiles have shown a reduction in the presence of the typical strong low-level inversion, due simply to surface warming eroding the cap itself. Further, once the cap is broken, the ascent of a standard parcel of air then follows more closely with a moist adiabatic ascent profile than it would have in the past. In our study, we examined several specifically chosen locations

over our three eras in order to illustrate certain changes. First, we highlight three islands along the North Atlantic storm track. Historically, this is the area where the highest frequency of convection occurs north of 60 °. Next, we discuss the changes over the Canadian Arctic Archipelago. Finally, we discuss a region of mean vertical temperature profiles for several areas where saturation potential vorticity has made a relatively extreme change between the three eras.

Greenland's unique location makes for intense convective activity. It is on the north end of the Gulf Stream, but the south end of Arctic air masses. The island itself is divided down the middle by a mountain chain. Upper level wind flow naturally approaches from the west, and the ascending air on the windward side of the mountain provides the dynamics for upper-level vorticity generation. The potential vorticity advection on the east side of the mountains meets with an atmospheric profile where cold air aloft is on top of the relatively warmer Gulf Stream waters, and all the ingredients for convection exist: moisture and lift.

4.4 North Atlantic Storm Track

Iceland is in the unique geographic position where the island serves as a boundary of sorts between the warm Gulf Stream waters and the cold Arctic waters to the north. Warm water pushes north from the east coast of North America to the point where it is sufficiently cooled by cold Arctic air masses, such that surface water density increases before sinking. This is the start of the deep ocean conveyor (Broecker, 1991). Figure A.5 shows the vertical temperature profile for Iceland over the three eras during the winter months December, January, and February (henceforth known as DJF). The blue (last glacial maximum) shows the classic Arctic stable temperature profile, with a strong near-surface inversion followed by a stable ascent relative to a moist adiabat up to the tropopause. Figure A.6 shows the three profiles for Jan

Mayen. The small island is roughly 5 ° north of Iceland, and exhibits a similar last glacial maximum profile. Subtle differences in the profiles lie in the mid-Holocene and 20th century profiles over the islands.

The red and green profiles in Figure A.5 for the mid-Holocene and 20th century, respectively, show a tremendous difference relative to the last glacial maximum. The mean vertical temperature profile over Iceland in the mid-Holocene and the 20th century does not show a low-level temperature inversion. This makes the region susceptible to convection, whereas historically, this has not been the case. While the ascent is stable relative to a moist adiabat, it is less stable than that of the last glacial maximum profile. Red and green profiles for both Iceland (Figure A.5) and Jan Mayen (Figure A.6) show that surface temperatures had increased enough to eliminate a mean surface inversion over Iceland by the mid-Holocene, but the inversion still existed over Jan Mayen. By the 20th century, both surface inversions were gone. Figure A.7 shows a vertical temperature profile of an area northwest of Jan Mayen. The southern tip of the Svalbard island shares the complete erosion of its inversion cap with Iceland and Jan Mayen, but despite being much further north than the other two islands, Svalbard shows more of a moist adiabatic profile than the other two.

4.5 Canadian Arctic Archipelago

Vertical temperature profiles over the Canadian Arctic Archipelago, the broken chain of islands surrounded by Baffin Bay, the Arctic Ocean, and the Beaufort Sea, show another interesting change between the three eras.

Figure A.8 is a profile taken over land in northern Canada. This figure shows that the last glacial maximum surface temperature was at roughly the 700 hPa level, meaning a thick ice sheet covered the surface. The ice sheet melted over the next

fifteen thousand years, showing the surface at the 900 hPa level, but the surface temperature responds in several interesting ways. The surface temperature is 10 °C higher by the mid-Holocene, and the 20th century profile is very similar to the mid-Holocene. While the mean profile is still stable, both profiles follow more closely with a moist adiabatic profile than during the last glacial maximum period.

Moving northward 5 ° latitude per figure, Figures A.9, A.10, A.11, and A.12 show warming at every level of the troposphere. Figures A.11 and A.12 are completely over water. These profiles show a warming surface and a vertical temperature profile relatively moist as compared to the past.

4.6 Regions with High P* Differences

In the next chapter, we will discuss the results of our P* diagnostic. For now, consider that there are two areas in the northern hemisphere where extreme differences in P* between the three eras exists: The North Atlantic storm track and the east coast of North America. Each region saw changes for different, but not unrelated, reasons. The coastal region was the result of large temperature swings on the east coast of large land masses. As cold air passes over a land mass, the surface changes the temperature of the air mass relatively quickly. This led to enhanced convection, further warmed the Gulf Stream waters and worked its way north into the storm track.

Within these regions, mean DJF vertical temperature profiles were constructed, limiting the North Atlantic storm track region to $60 - 80\,^{\circ}\mathrm{N}/0 - 50\,^{\circ}\mathrm{E}$ and the east coast of North America was limited to $50 - 60\,^{\circ}\mathrm{N}/60 - 10\,^{\circ}\mathrm{W}$. The storm track (Figure A.13) shows that once the low-level inversion cap is broken, the mean profile of the air has changed over time to where it follows nearly entirely along a moist adiabat up to the tropopause. The North American coast (Figure A.14) shows an

extremely shallow low-level inversion, but surprisingly, the mid-Holocene and 20th century cases show almost the exact same stability profile as that of the last glacial maximum.

One interesting note is that the level of the tropopause appears to rise with time over the three eras in each profile examined in this section, except for the first two Canadian Archipelago cases where the profile was taken entirely over land at the origin of the cold Arctic air mass (Figures A.8 and A.9). Another important note: none of the vertical temperature profiles examined in this section show 500 hPa temperatures below $-45\,^{\circ}\mathrm{C}$.

5. MINIMUM MID-TROPOSPHERIC TEMPERATURES

Chase et al., 2002; Tsukernik et al., 2004; Herman et al., 2008 found in a study of modern observations that in spite of surface temperatures falling well below, and 500 hPa temperatures reaching these levels by mid-November, 500 hPa temperatures very rarely fell below −45 °C, and never fell below −47.5 °C in any given season. In an expansion of this project, we reviewed CCSM4 and NCEP/NCAR data to verify this during different periods of time.

Our study utilized 6-hourly temperature data from CCSM4 model runs and NCEP/NCAR reanalysis. This data was separated into bins of several different values in order to assess the overall environment. Bins were created for −40 °C, −42.5 °C, −45 °C, and −47.5 °C, while Chase et al., 2002; Tsukernik et al., 2004; Herman et al., 2008 created figures for −40 °C, −42 °C, and −44 °C. Each time the threshold was met, that bin was filled with a one. Logically, the −40 °C bin included every value below, to include those in other bins, so the results from the four bins are cumulative. The −40 °C figure shows the largest total area, with −42.5 °C smaller and −45 °C the smallest and −47.5 °C showing zero. The total area below each threshold was tallied and recorded for each month of the period examined.

5.1 NCEP/NCAR Area

The NCEP/NCAR reanalysis includes data from 1948-2013, similar to the project accomplished by the authors in Chase et al., 2002; Tsukernik et al., 2004; Herman et al., 2008. First, as a sanity check with respect to previous work, we conducted a pseudo-verification of their results using NCEP/NCAR data for the 20th century. Figures A.15, A.16, and A.17 show the NCEP/NCAR reanalysis model results within the framework of our experiment. The results closely resemble those of the authors

in the previous studies, which used observational data in addition to reanalysis data.

The total surface area in the Arctic (north of 60 °N) within our grid is 3.5571x10^7km^2. Figure A.15 shows the 1950s with a maximum total area below −40 °C at the 500 hPa level of 1.8x10^7km^2, which is roughly half the total area of the Arctic. Figure A.16 shows the total area below −42.5 °C drops to approximately 1x10^7km^2 in the 1950s, and is near zero by present day. This agrees with our atmospheric temperature profiles from the previous chapter, where 20th century 500 hPa temperatures rarely fell below −42.5 °C. Figure A.17 is the root of this paper, and it shows that there are only two periods in the NCEP/NCAR reanalysis where the temperature at 500 hPa falls below −45 °C: the early 1950s and the late 1970s. Even still, total area below −45 °C in the early 1950s does not exceed 0.2x10^7km^2 and 0.35x10^7km^2 in the late 1970s, which is less than 6% and 10% of the total area respectively. Several ebbs and flows exist within this time frame, with relatively colder periods aloft in the early 1950s, mid 1960s, late 1970s, late 1980s, and mid to late 1990s. Present day simulations show no strong trend over the period except, perhaps, in the final decade, when area below −40 °C is smaller for a longer interval than earlier (areas this low were recorded before, but usually were interspersed between other years with larger areal extent of −40 °C).

5.2 CCSM4 Area

In Chase et al., 2002, the authors called for further examination of the work on mid-tropospheric temperature regulation using model data. For reasons mentioned previously, this section will highlight the results of the same three eras from previous sections using CCSM4 model data. One important note is that the years on the y-axis of each figure are model years within the simulations themselves, not years on the modern calendar.

In the 20th century, especially after the 1950s, climatic warming became dramatic (Yao et al., 1997). The 20th century CCSM4 model run gives us another look at the modern era. Figure A.18 shows the area below $-40\,^{\circ}$C. The maximum values reach 1.5x10^{7}km^2 in February during several different years. Comparing the results to the NCEP/NCAR reanalysis (Figure A.15), we see that the maximum area over the period does not exceed 1.8x10^{7}km^2. In Figure A.19, we see the Arctic area below $-42.5\,^{\circ}$C. The maximum area in this plot does not exceed 1x10^{7}km^2 in only a few very sparse times. The rest of the plot shows an area of zero. Lastly, Figure A.20 shows the area below $-45\,^{\circ}$C. In the 20th century CCSM4 model run, there is not a single data point on the grid north of the Arctic circle where 500 hPa temperature falls below $-45\,^{\circ}$C. The NCEP/NCAR reanalysis (Figure A.17) shows a maximum area below $-45\,^{\circ}$C of roughly 0.3x10^{7}km^2, which is the same difference noticed between the $-40\,^{\circ}$C plots between the two model runs.

During the last glacial maximum, the Arctic surface was almost entirely ice, both on land and ocean. It stands to reason that the temperature throughout the atmospheric profile would be colder than $-45\,^{\circ}$C. Examination of the last glacial maximum, Figure A.21, shows that for the most part, the entire area at 500 hPa is below $-40\,^{\circ}$C during the winter months. The proposed mid-tropospheric regulatory mechanism of Arctic air masses coming into contact with open ocean was not as consistent, as there were simply less opportunities for such occurrences. Figure A.22 shows that a substantially smaller area below $-42.5\,^{\circ}$C exists during the winter. Interestingly, while Figure A.23 still shows roughly 30% of the total area below $-45\,^{\circ}$C in the winter months, examining Figure A.24 shows us that despite omnipresent ice, there is no appreciable area below $-47.5\,^{\circ}$C, although surface temperatures during the last glacial maximum averaged $-37\,^{\circ}$C. We will examine the reasons for this in section six.

The mid-Holocene case is much more closely related to the modern era. The atmosphere contained preindustrial era carbon dioxide levels (roughly 280 ppm), and similar methane levels (650 ppb in the mid-Holocene, versus 760 ppb post-industrial), but the seasonal cycle of solar radiation changed the amount of solar radiation going into and coming out of winter darkness periods. Figure A.25 shows the total area below $-40\,^{\circ}$C. Compared to Figures A.21, A.22, A.23, and A.24 of the last glacial maximum, we immediately notice a sharp contrast in the magnitude of this plot. The maximum area below $-40\,^{\circ}$C is approximately $2.2\text{x}10^7\text{km}^2$ in February late in the model run. Figure A.26 shows the area below $-42.5\,^{\circ}$C, with a maximum area of approximately $1.5\text{x}10^7\text{km}^2$ at roughly the same time as the maximum area in the $-40\,^{\circ}$C plot. And finally, Figure A.27 shows the area below $-45\,^{\circ}$C, with a maximum area of just below $1\text{x}10^7\text{km}^2$ in only a few sparse times. The rest of the time, the area is zero. Interestingly enough, this period shows an areal plot similar in magnitude at $-40\,^{\circ}$C (Figure A.25) to the $-45\,^{\circ}$C plot (Figure A.23) from the last glacial maximum period. In the winter months, roughly 30% of the total area is below $-40\,^{\circ}$C in both cases. This is simply an indication that the mid-Holocene was an era where Arctic air masses had relatively unimpeded access to open ocean surfaces, which is supportive of the proposed mechanism for mid-tropospheric temperature regulation. Ultimately, the mid-Holocene model data figures are very similar to those of the NCEP/NCAR reanalysis from the satellite era (Figures A.15, A.16, and A.17), despite being six-thousand years earlier.

The surface during the last glacial maximum was much colder than that of the surface during the mid-Holocene or the 20th century. Therefore, it should be expected that the upper levels of the atmosphere during the last glacial maximum are colder as well. A difference does in fact exist, but it is not to the same degree as you can typically expect in a typical column of air. While Figure A.23 shows us a significant

last glacial maximum area below $-45\,^{\circ}$C as compared to the other two eras, it is almost more important to consider the substantial drop from roughly 30% of the total area below $-45\,^{\circ}$C to almost 0% below $-47.5\,^{\circ}$C (Figure A.24). This suggests that the proposed regulatory mechanism is at work, although it has more of an uphill battle to maintain temperatures consistent with a moist adiabatic process. The 20th century model run is unique to this study, in that it gave us a third look at the modern era, considering the NCEP/NCAR figures and the work of Chase et al., 2002; Tsukernik et al., 2004; and Herman et al., 2008. The Chase et al., 2002 paper shows the total area of the Arctic below the $-44\,^{\circ}$C isotherm, whereas our NCEP/NCAR reanalysis and CCSM4 20th century cases show the area below the $-45\,^{\circ}$C isotherm. All three cases show an area no greater than $0.3\text{x}10^{7}\text{km}^{2}$ at $-44\,^{\circ}$C and $-45\,^{\circ}$C respectively, and all three cases show such occurrences to be for very short, and sparse, periods of time. This study concludes that no more than 1% of the Arctic fell below $-45\,^{\circ}$C at the same time, in only the NCEP/NCAR reanalysis during three times during the model run.

6. SATURATION POTENTIAL VORTICITY AND TRANSIENT EDDY FLUX

We now examine some reasons for the absence of temperatures colder than −45°C in the middle tropospheric Arctic winter. In a pioneering paper, Curry (1983) noted some of the unexpected thermodynamic properties in polar air masses that included cooling at rates exceeding those of simple radiative models. (She showed a progression of soundings from Fairbanks, Alaska, in December 1961 that showed lower tropospheric cooling of more than 30°C in less than two weeks. Advection from other areas can be ruled unlikely on the basis of concurrent data from reanalysis and other stations, and the fact that this was the formation of an anomalous cold pool of air.) Curry (1983) noted that timescales for the formation of Arctic air in radiative codes were particularly sensitive to the small amounts of water present at these low temperatures. Even though moist convection is nearly absent over these polar continents during winter (Korty and Schneider 2007), residual moisture transported from other areas can have a profound effect throughout the Arctic.

6.1 Saturation PV

As introduced in Section 2, saturation potential vorticity (P*) shows how θ_e^* changes along surfaces of angular momentum. As moist adiabats are defined by constant values of θ_e^*, wherever P* is zero a moist adiabatic lapse rate exists along an angular momentum surface. (Angular momentum surfaces are nearly vertical in practice, though in strongly rotating systems they can deflect laterally. Thus this quantity captures both upright vertical convection as well as symmetric instabilities during those times and places where convective ascent occurs over slanted pathways [e.g., frontal boundaries].)

Regions with direct access to large bodies of water tend to show more of a moist

adiabatic profile than those without direct access. Near the tropics, for example, stability will typically be more or less conditionally unstable, with a profile following a moist adiabat more often than not, and the chances of such occurrence decrease as you move away from warmer temperatures and available moisture toward the colder, relatively dry poles. The intent of this diagnostic tool is to couple with vertical temperature profiles in order to illustrate that an area with near-zero or negative saturation potential vorticity values have seen recent convection. Because convection in the Arctic is non-standard in the sense that strong low-level inversions typically limit convection, this tool shows us convection as calculated on a slanted angular momentum surface.

The environment is changing, and it is important to highlight the differences in the climate between various time periods. The last glacial maximum was a period where earth was in roughly the same phase of its orbital procession as it is today, but the climate was much colder as the ice sheet extended south over the landmasses of the northern hemisphere. The mid-Holocene case gives us a time period where the climate was similar to ours today, as there was no ice sheet, but six thousand years ago the orbital procession of earth was out of phase with our current orbit. Thus in the mid-Holocene, the earth was closest to the sun in July, whereas today, earth is closest to the sun in January. Climatologically, this gives us two distinct cases where the climate is controlled by different factors: incoming solar radiation and ice.

Because saturation potential vorticity values are very small, typically on the order of 10^{-6} practical vorticity units, all of our figures and calculations have been made after first multiplying the P* values by 10^6 so that values are order of one. This gives us the ability to quickly assess the environment; positive, negative, or near-zero. In the tropics, we could calculate mean values from any number of data sets, but in the Arctic, it is important to remember that convection is infrequent and such

occurrences of convection would be lost in virtually any mean calculation. Thus requiring a different approach with respect to data collection in order to assess the environment using the P* diagnostic.

In order to best capture the occurrence of Arctic convection, we used six-hourly CCSM4 data. This makes it possible to capture specific events versus relying on data with lower temporal resolution. The data is first separated into bins specific to the experiment. The first experiment separated data into P* < -0.15, -0.15 < P* < 0.15, and P* > 0.15 (unstable with respect to moist convection, nearly neutral, and stable). The bins are then summed with a maximum possible value of four times per day times number of days per month times number of years in each simulation. The results are normalized by dividing by the total number of days in each simulation to make for an easy comparison between time periods of varying length. In order to best illustrate the changing Arctic environment, the bins bifurcated data into P* < 0.15 and P* > 0.15, thus lumping the cases with neutral and lower stability into a single group (all cases in this bin may have some signature of convectively adjusted profiles). Because their vertical temperature profiles are very similar, this makes it possible to see what we need for our purposes. For example, Figure A.28 illustrates a vertical temperature profile north of the Arctic Circle, in this case located in Iceland, where P* is zero from the surface throughout the troposphere. The sounding shows no surface inversion and its ascent follows a moist adiabat up to the tropopause. Ultimately, the P* diagnostic allows for a quick, easy glance into the environment, affording us the ability to make a diagnosis of the state of the column of air represented.

6.2 Cross-sectional P*

Cross-sections of P* over the three eras provide additional insight into the northward extent of convection in the Arctic. During the last glacial maximum, Figures

A.29, A.30, and A.31 show cross-sections from 60, 70, and 75 °N. At this time, the ice sheet over North America was so thick that the surface pressure was elevated into the 600-700 hPa ranges. To the east of the ice sheet, the North Atlantic storm track is where the majority of occurrences where P* approaches zero occur. At 60 and 65 °N, P* approaching zero reaches maximum occurrence levels over the storm track. At 70 °N, however, all P* throughout the Arctic is limited such that the mean environment is stably stratified. Stable stratification is to be expected as you approach the north pole for several reasons, specifically a lack of availability of water vapor at high latitudes during this time period and the absence of available heating sufficient to break the low-level inversion.

In each of the three eras, we can see the prevalence of a wave number two pattern across the northern hemisphere. Areas where mean P* approaches zero exist over the North Atlantic storm track and over the Bering Strait. In the mid-Holocene, Figures A.32, A.33, and A.34 show big changes in the occurrence of P* approaching zero, especially over the North Atlantic storm track, as well as at an elevated level over northern Canada at 60 °N. The ice sheet has melted, and the surface is exposed to higher amounts of incoming solar radiation during this period specifically, as earth is physically closer to the sun during the summer months. Because the land heats up more quickly than its ice sheet predecessor, elevated areas where P* approaches zero are expected to be more prevalent, and the aforementioned figures show such a situation. This interesting phenomena ceases to exist at higher latitudes.

In the 20th century, Figures A.35, A.36, and A.37 show mean winter P* values approaching zero at each latitude band over the North Atlantic storm track and the Bering Strait. In these areas, values are more close to zero than at any other point or location in any other era. Differences in conditions exist between the three eras such that each era shows progressively stronger P* signatures approaching or below

zero throughout the Arctic. In the last glacial maximum, P* values approaching or below zero were only significant up to about 450 hPa at 70 °N, whereas in the mid-Holocene and the 20th century, P* was significant up to about 400 hPa at 70 °N. The P* signature in the 20th century suggests that P* approaches zero up to about the 350 hPa level at 60 °N.

6.3 Last Glacial Maximum - 20th Century Differences

Taking a difference of the normalized six-hourly P* occurrences between the last glacial maximum and the 20th century gives us a broad overview of the changes between the periods. The data is six-hourly taken from CCSM4, which was combined into bins where P* values < 0.15 and then > 0.15 were summed over the entire time period. This information was normalized by dividing by the total number of days in each time period. The maximum fluctuation in number of occurrences per day is +/- 4. This indicates entire areas which saw zero occurrences of P* at or below 0 became areas that saw four occurrences in any one day. For example, Figure A.38 shows us the last glacial maximum - 20th century, where the maximum upward swing in P* occurrence <0.15 is roughly 0.5 more per day over Scandinavia.

The North Atlantic storm track generally shows an increase of nearly 0.5 more occurrences per day at 775 hPa in the 20th century than during the last glacial maximum. Figure A.39 shows a change of roughly 0.3 more occurrences per day at 550 hPa over North America, with between 0.1-0.2 more occurrences over the North Atlantic storm track and off the northeast coast of Japan. Figure A.40 shows 350 hPa, which is approximately the level of the jet stream. Here, we see the most extreme changes between the two periods. While the maximum swing is no more than 0.2 more occurrences per day, the entire map illustrates a higher magnitude with respect to the difference between the two lower levels mentioned above. The

only area without a notable upswing in occurrences of P* <0.15 per day is between eastern Eurasia and the Rocky Mountains.

6.4 Mid-Holocene - 20th Century Differences

The important difference between these two eras is in the seasonal cycle. The ice age has been over for some time, and the mid-Holocene receives more direct solar radiation than the 20th century in the northern hemisphere. Still, the 20th century sees a higher frequency of occurrence of convection than the mid-Holocene, as evidenced by a higher frequency of P* occurrences near or below zero at higher latitudes and at higher elevations than in any other time in earth's history.

Normalized differences in six-hourly P* occurrences between the mid-Holocene and the 20th century show increases on a smaller scale than those of the last glacial maximum to the 20th century. At 775 hPa, Figure A.41 shows that the 20th century sees an increase of roughly 0.1 occurrences per day on average in the winter time over the North Atlantic storm track and the Bering Strait region. Figures A.42 and A.43 show us that at 550 and 350 hPa, the Canadian Arctic Archipelago is the region where the biggest difference between the eras is seen. As mentioned in the cross-sectional P* section, this is an area experiencing a tremendous amount of change with the melting ice sheet and transforming landscape. Northern Eurasia shows a similar P* signature to its North American counterpart.

Examining cross-sections and differences between P* spatially and temporally at three different latitude bands over three distinct eras suggests that the Arctic is becoming more tropical over time. The frequency of convection is increasing, and the location of such convection is pushing further north. These occurrences should be expected to feed into a positive feedback mechanism, such that convection increases cloud cover, which further melts the ice, which increases the availability of water

vapor, thus increasing the duration and strength of convection itself. And then the process repeats.

6.5 NCEP −45 °C Areal Anomalies

Figure A.17 shows the total area in the Arctic where temperatures fall below −45 °C. Two times stand out as anomalies: January 1951 and February 1979. During these months, there are significant areas where upwards of 3.5x$10^6 km^2$ saw temperatures below −45 °C. Figures A.44 and A.45 show P* at 775 and 550 hPa respectively for the month before, month of, and month after the January 1951 cold temperature anomaly at 500 hPa. In December, the Arctic shows mostly positive PVU values. There are no areas where significant convection occurs. This represents a departure from the mean (Figures A.35, A.36, and A.37), where the storm tracks typically show negative PVU values of P* during the winter months. In the last panel of each figure, February, we see a strong convective signature with large areas of negative P* values. By March 1951, there are no regions where 500 hPa temperatures fall below −45 °C.

Figures A.46 and A.47 show the 775 and 550 hPa levels for the month before, month of, and month after the February 1979 cold temperature anomaly at 500 hPa. In January, the Arctic shows mostly positive PVU values. Like the January 1951 case, there are no areas where significant convection occurs, which represents a departure from the mean. In February, convective activity picks up in the storm tracks and this continues in March. An interesting contrast between the two cases is that while Figures A.44 and A.45 showed strong convection in the February 1951 panel, Figures A.46 and A.47 showed no strong areas of convection, rather a weakening of areas where strong stability existed. Additionally, convective activity increases south of the Arctic. This shows that broad areas of marginally increased convection had the same

effect as one area with significantly increased convection on the mid-tropospheric temperature.

6.6 Mid-latitude and Arctic Heat Flux

The Arctic is a region of the planet where a tremendous energy deficit exists. North of the Arctic Circle, the region experiences twenty four hour periods of darkness throughout winter. Because solar radiation drives many of the physical mechanisms and processes on earth, the region requires an influx of energy from outside the region to maintain mean temperatures. Meridional heat fluxes are necessary to balance the energy budget on the planet. Extra-tropical regions transport heat northward into the Arctic with the atmosphere dominating the contributions of the oceans at these latitudes. Because northward heat transport is prevalent, we are interested not only in the Arctic, but in the regions to the near-south as well. We break the total sensible heat transport (A below) into contributions from mean and eddy fluxes.

$$\underbrace{\overline{VT}}_{A} = \underbrace{\overline{V}\,\overline{T}}_{B} + \underbrace{\overline{V'T'}}_{C} \tag{6.1}$$

"A" is the total meridional sensible heat flux, "B" is the mean flux, and "C" is transient eddy flux. The third term is of particular interest to us because a positive departure in transient eddy flux represents a positive departure from the time-averaged meridional (north/south) wind and temperature (Serreze and Barry, 2005). CCSM4 model data was used to examine data throughout three eras: the last glacial maximum, mid-Holocene, and 20th century, and results are discussed below.

During the last glacial maximum, Figure A.48 shows the mean November through March transient eddy heat flux into and out of the region at 500 hPa. The region is mostly near-zero, with the exception of several relatively strong positive flux areas: the North Atlantic storm track, an area of eastern Eurasia, eastern China, and the

east coast of Japan. The storm track sees a maximum value of 25 K*m/s. This area is broad, ranging from the Great Lakes of North America northeast through the west coast of Scandinavia. The east coast of Japan is the second most active region shows nearly 20 K*m/s. This positive flux area is similar to that of the storm track region, but on a smaller scale. The significant positive flux area does not extend into the Aleutian islands. Eastern China shows roughly 15 K*m/s. This area is the smallest region, limiting itself to near-tropical regions of present-day Shanghai. The east coast of Greenland saw an average of approximately 12 K*m/s. Eastern Greenland is an area of enhanced convective activity largely due to convective activity associated with positive vorticity advection on the leeside of the mountain chain, which divides Greenland down the center. Eastern Eurasia shows a maximum value of roughly 10 K*m/s. Like Greenland, this region is likely an extension of the Gulf Stream moving northward in the Atlantic. The two most active positive transient eddy flux regions of the northern hemisphere during the last glacial maximum tend to follow the Gulf Stream and the Kuroshio Current.

Northward heat transport is accomplished either by northward advection of warm air or southward transport of cold air. Because the data uses temperature values in Kelvin, the negative component of the meridional winds means a southward transport of relatively cold air out of the Arctic, thereby making the region warmer. Each strongly positive transient eddy flux region has a corresponding strongly negative couplet. The Gulf Stream/eastern Greenland positive region has a negative couplet over the Canadian Arctic Archipelago, with values in the -15 K*m/s range. The region was covered with an ice sheet and Arctic air masses pushed south into North America during the last glacial maximum. The eastern Eurasia couplet is to the southwest over Europe, with values in the -10 K*m/s range. The eastern China/Kuroshio couplet is to the northwest in Siberia, with an extreme value in the -12 K*m/s range. The Gulf

Stream positive transient eddy flux region is so strong, a secondary negative couplet exists in the American southwest, with values in the -12 K*m/s range. None of the couplets are as strong as their positive counterpart.

Figure A.49 shows the mid-Holocene mean November through March transient eddy heat flux into and out of the region at 500 hPa. Like the last glacial maximum, the Arctic is typically near-zero, with areas of enhanced strong positive eddy flux regions. The Gulf Stream shows a maximum positive transient eddy flux region in the range of 25 K*m/s, extending from the Great Lakes region of North America further north than its last glacial maximum counterpart to the Svalbard islands north of Scandinavia. The core of the maximum strength is centered farther south than in the last glacial maximum, but the overall area reaches farther north. With the ice sheet melted, the primary negative couplet for this positive region is in the American Southwest. Negative values are in the -5 K*m/s range. The same is true for the Kuroshio region off the east coast of Japan. Maximum positive transient eddy flux values reach into the 20 K*m/s range, but the region extends beyond the Aleutian Islands, through the Bering Strait, and the west coast of North America. Its negative couplet exists over Siberia in the -10 K*m/s range.

Figure A.50 shows the 20th century mean November through March transient eddy heat flux into and out of the region at 500 hPa. Similar to the previous two eras, the 20th century couplets are in roughly the same regions, with roughly the same values as that of the mid-Holocene. An interesting difference between the last glacial maximum and the two more recent eras exists over Greenland. During the last glacial maximum, the east coast of Greenland was an area of enhanced positive transient eddy flux. During the mid-Holocene and 20th century, however, that region shifted inland and to the southern tip. This still makes physical sense, as the areas are still east of the mountain range. Observational data shows that today, Greenland

sees enhanced convective activity at the southern tip during winter months.

Figure A.51 shows two figures. The top figure shows the difference in transient eddy heat flux between the last glacial maximum to the 20th century, and the bottom figure shows the difference between the mid-Holocene and 20th century. Strong positive flux differences in the range of 15-20 K*m/s exist between the last glacial maximum and 20th century exist over Alaska, the Canadian Arctic Archipelago, southern Greenland and the northern Scandinavia/Svalbard Islands region. Between the mid-Holocene and 20th century, small positive flux differences in the range of 2-4 K*m/s exist over eastern Europe, the Kuroshio current, Canadian Arctic Archipelago, eastern North America, and over the North Atlantic storm track. There are no noticeable areas of negative flux differences.

Table B.2 shows the total transient eddy heat flux differences between the last glacial maximum and the 20th century and the mid-Holocene and the 20th century. The first row shows the northern hemisphere difference, north of 30 °N and the second shows only the Arctic, which we've defined as the region north of 60 °N. The total differential transient eddy heat flux over the northern hemisphere between the last glacial maximum and the 20th century is -2.8534x10^7J kg^{-1} m/s, and over the Arctic is -1.8866x10^7J kg^{-1} m/s. Between the mid-Holocene and 20th century, the difference is -3.1476x10^6J kg^{-1} m/s over the northern hemisphere and -2.6216x10^6J kg^{-1} m/s over the Arctic.

7. SUMMARY AND CONCLUSIONS

In previous works, several groups explored the possibility of a mid-tropospheric temperature regulation mechanism. Chase et al., 2002; Tsukernik et al., 2004; Herman et al., 2008 showed that temperatures in the mid-troposphere reached $-45\,^{\circ}\mathrm{C}$ by mid-November, but very rarely fell below. This was true even through the winter months, where incoming solar radiation ceases to exist entirely. Overwhelming support exists for a moist-adiabatic temperature regulation process, as $-45\,^{\circ}\mathrm{C}$ corresponds to a surface temperature of approximately $-2\,^{\circ}\mathrm{C}$, just about the freezing temperature of high-latitude seawater. We explored several mechanisms concerning the feasibility of open-ocean coming into contact with Arctic air masses. Most importantly, our study expanded upon previous works by looking into paleoclimate via CCSM4, NCEP/NCAR.

Because the proposed mid-tropospheric temperature regulation mechanism relies on open ocean, sea ice is an impediment. August and September are the months where the annual extreme minimum sea-ice coverage exists in the northern Hemisphere. Since Arctic sea ice reached its lowest areal extent in the satellite record in September 2007, measuring 40% below the long-term mean (Comiso et al., 2008), the last six years (2007-2012) have witnessed the six lowest September sea ice extents in the modern record (Screen and Simmonds 2013). The significance is that less sea ice means more open ocean, which provides a positive feedback mechanism for the changes analyzed in this study. More open ocean surfaces provide an interface for Arctic air masses to interact more freely with relatively warmer surface waters, thus changing the vertical temperature profile of the atmosphere entirely.

Skew-T log-p diagrams taken from several locations north of the Arctic circle show

a changing vertical temperature profile such that temperatures are warming and their profiles are becoming more moist adiabatic. Additionally, warming surface temperatures are eroding the strength of typically strong low-level temperature inversions in the Arctic. A small modification to Equation 2.1, the Ertel (1942) potential vorticity equation, by Emanuel (2008) in Equation 2.2, uses saturation equivalent potential temperature (θ_e^*) in place of virtual potential temperature (θ). This allowed us to quickly assess the convective environment via model data throughout three distinctly unique eras. Differences in saturation potential vorticity between the last glacial maximum and the 20th century, and between the mid-Holocene and the 20th century revealed that the 20th century is the most convectively active time period over the last twenty-one thousand years. The ultimate conclusion is that moist-adiabatic characteristics of a tropical environment are progressing northward over time into the Arctic.

Using CCSM4 model data and NCEP/NCAR reanalysis data, we explored changes in the 500 hPa area where the temperature dropped below $-45\,^{\circ}$C. First, we explored the last glacial maximum, a period in time where earth was physically in the same location in its procession as it is at present. Over an era where the northern hemisphere was almost entirely covered with ice, mid-tropospheric temperatures were still regulated to within no more than a couple degrees of $-45\,^{\circ}$C during the most extreme cold occurrences during the period. Next, the mid-Holocene afforded us a glimpse into a period where earth's perihelion occurred during the summer, versus modern day winter. The climate was very similar, as the ice sheets over North America and Eurasia had largely melted away, but there was an increased amount of incoming solar radiation incident upon the surface. During this period, mid-tropospheric temperatures never fell below $-45\,^{\circ}$C for any extended period of time, and did not fall below $-47.5\,^{\circ}$C once. Finally, we were fortunate to be able to see the 20th century

through several different lenses: the CCSM4 model run, NCEP/NCAR reanalysis, and previous works involving real-time observations. NCEP/NCAR and CCSM4 confirmed the findings of previous authors, with NCEP/NCAR showing only a small number of occurrences where the temperature fell below $-45\,^{\circ}\mathrm{C}$, and CCSM4 showing exactly zero occurrences.

The Arctic is warming at all levels of the troposphere. Transient eddy flux at the 500 hPa level showed increasing eddy flux over the northern hemisphere during the three eras. Because seasonality is important, we extended our winter months to include November and March, including the transition periods where the Arctic was going into and coming out of 24 hour periods of darkness. Regions of positive and negative transient eddy flux have remained roughly the same over the last twenty one thousand years, as has magnitude of the flux itself. The regions of positive flux appear to be expanding, while the regions of negative flux appear to be shrinking in both size and magnitude. Increases in transient eddy heat flux, and northward intrusion of positive values indicate that convective processes are intruding northward in the northern hemisphere over time.

The views expressed in this thesis are those of the author, and do not reflect the official policy or position of the United States Air Force, Department of Defense, or the U.S. Government.

REFERENCES

Broecker, W. S. et al., 1991: The great ocean conveyor. *Oceanography*, **4 (2)**, 79–89.

Chase, T., B. Herman, R. Pielke, X. Zeng, and M. Leuthold, 2002: A proposed mechanism for the regulation of minimum midtropospheric temperatures in the arctic. *Journal of Geophysical Research: Atmospheres (1984–2012)*, **107 (D14)**, ACL–2.

Clement, A. C., R. Seager, and M. A. Cane, 2000: Suppression of el niño during the mid-holocene by changes in the earth's orbit. *Paleoceanography*, **15 (6)**, 731–737.

Collins, W. D., et al., 2006: The community climate system model version 3 (ccsm3). *Journal of Climate*, **19 (11)**, 2122–2143.

Comiso, J. C., C. L. Parkinson, R. Gersten, and L. Stock, 2008: Accelerated decline in the arctic sea ice cover. *Geophysical Research Letters*, **35 (1)**, 1–6.

Curry, J., 1983: On the formation of continental polar air. *Journal of the Atmospheric Sciences*, **40 (9)**, 2278–2292.

Curry, J. A., J. L. Schramm, and E. E. Ebert, 1995: Sea ice-albedo climate feedback mechanism. *Journal of Climate*, **8 (2)**, 240–247.

Emanuel, K., 2008: Back to norway: An essay. *SynopticDynamic Meteorology and Weather Analysis and Forecasting*, Cambridge, Massachusetts USA: Springer., 87–96.

Emanuel, K. A., 1983: The lagrangian parcel dynamics of moist symmetric instability. *Journal of the Atmospheric Sciences*, **40 (10)**, 2368–2376.

Ertel, H., 1942: Ein neuer hydrodynamischer wirbelsatz. *Meteorol. Z.*, **59**, 277–281.

Fang, Z. and J. M. Wallace, 1994: Arctic sea ice variability on a timescale of weeks and its relation to atmospheric forcing. *Journal of Climate*, **7 (12)**, 1897–1914.

Francis, J. A., W. Chan, D. J. Leathers, J. R. Miller, and D. E. Veron, 2009: Winter northern hemisphere weather patterns remember summer arctic sea-ice extent. *Geophysical Research Letters*, **36 (7)**, 1–5.

Francis, J. A. and S. J. Vavrus, 2012: Evidence linking arctic amplification to extreme weather in mid-latitudes. *Geophysical Research Letters*, **39 (6)**, 1–5.

Frisius, T., 2005: An atmospheric balanced model of an axisymmetric vortex with zero potential vorticity. *Tellus A*, **57 (1)**, 55–64.

Gent, P. R., et al., 2011: The community climate system model version 4. *Journal of Climate*, **24 (19)**, 4973–4991.

Hansen, J., R. Ruedy, M. Sato, and K. Lo, 2010: If it is that warm, how come it is so darned cold? *An Essay on Regional Cold Anomalies Within Near-record Global Temperature*, 1–14, online; accessed 30-November-2013.

Herman, B., M. Barlage, T. Chase, and R. Pielke, 2008: Update on a proposed mechanism for the regulation of minimum midtropospheric and surface temperatures in the arctic and antarctic. *Journal of Geophysical Research: Atmospheres (1984–2012)*, **113 (D24)**, 1984–2012.

Kalnay, E., et al., 1996: The ncep/ncar 40-year reanalysis project. *Bulletin of the American Meteorological Society*, **77 (3)**, 437–471.

Korty, R. L. and T. Schneider, 2007: A climatology of the tropospheric thermal stratification using saturation potential vorticity. *Journal of Climate*, **20 (24)**, 5977–5991.

Liu, Y., J. R. Key, Z. Liu, X. Wang, and S. J. Vavrus, 2012: A cloudier arctic expected with diminishing sea ice. *Geophysical Research Letters*, **39 (5)**, 1–5.

Morgan, H., 1945: The earth's perihelion motion. *The Astronomical Journal*, **51**, 127.

Njoku, E., 2004: SMEX03 AMSR-E Daily Gridded Soil Moisture and Brightness Temperatures. Tech. rep., NASA DAAC at the National Snow and Ice Data

Center, http://dx.doi.org/10.7265/N5. Boulder, Colorado USA. Online; accessed 2-October-2013.

Overpeck, J., et al., 1997: Arctic environmental change of the last four centuries. *Science*, **278 (5341)**, 1251–1256.

Rigor, I. G., J. M. Wallace, and R. L. Colony, 2002: Response of sea ice to the arctic oscillation. *Journal of Climate*, **15 (18)**, 2648–2663.

Schneider, T., 2004: The tropopause and the thermal stratification in the extratropics of a dry atmosphere. *Journal of the Atmospheric Sciences*, **61 (12)**, 1317–1340.

Screen, J. A. and I. Simmonds, 2010: The central role of diminishing sea ice in recent arctic temperature amplification. *Nature*, **464 (7293)**, 1334–1337.

Screen, J. A., I. Simmonds, C. Deser, and R. Tomas, 2013: The atmospheric response to three decades of observed arctic sea ice loss. *Journal of Climate*, **26 (4)**, 1230–1248.

Serreze, M., A. Barrett, J. Stroeve, D. Kindig, and M. Holland, 2009: The emergence of surface-based arctic amplification. *The Cryosphere*, **3 (1)**, 11–19.

Serreze, M. C. and R. G. Barry, 2005: *The Arctic Climate System*, Vol. 22. Cambridge, New York USA: Cambridge University Press.

Serreze, M. C. and J. A. Francis, 2006: The arctic amplification debate. *Climatic Change*, **76 (3-4)**, 241–264.

Simmonds, I. and K. Keay, 2009: Extraordinary september arctic sea ice reductions and their relationships with storm behavior over 1979–2008. *Geophysical Research Letters*, **36 (19)**, 1–5.

Stieglitz, M., S. Déry, V. Romanovsky, and T. Osterkamp, 2003: The role of snow cover in the warming of arctic permafrost. *Geophysical Research Letters*, **30 (13)**, 54–1–54–5.

Stone, P. H. and J. H. Carlson, 1979: Atmospheric lapse rate regimes and their

parameterization. *Journal of the Atmospheric Sciences*, **36 (3)**, 415–423.

Strong, C. and R. E. Davis, 2007: Winter jet stream trends over the northern hemisphere. *Quarterly Journal of the Royal Meteorological Society*, **133 (629)**, 2109–2115.

Tsukernik, M., T. N. Chase, M. Serreze, R. Barry, R. Pielke, B. Herman, and X. Zeng, 2004: On the regulation of minimum mid-tropospheric temperatures in the arctic. *Geophysical Research Letters*, **31 (6)**, 1–4.

Yao, T., Y. Shi, and L. Thompson, 1997: High resolution record of paleoclimate since the little ice age from the tibetan ice cores. *Quaternary International*, **37**, 19–23.

APPENDIX A

FIGURES

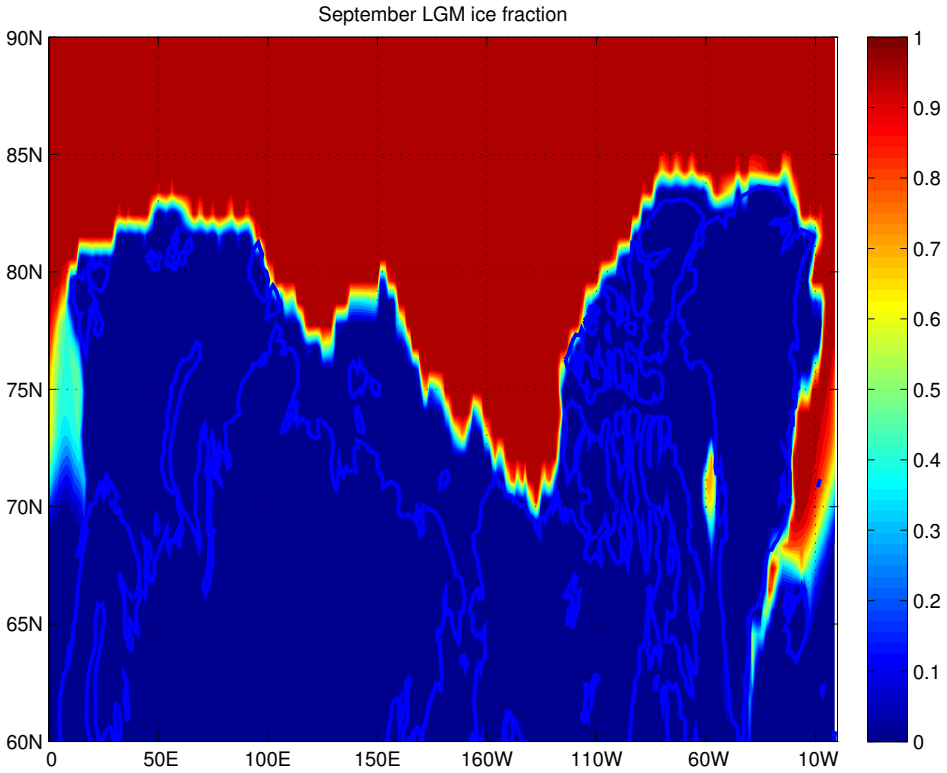

FIGURE A. 1. CCSM4 - Last Glacial Maximum September mean sea ice concentration

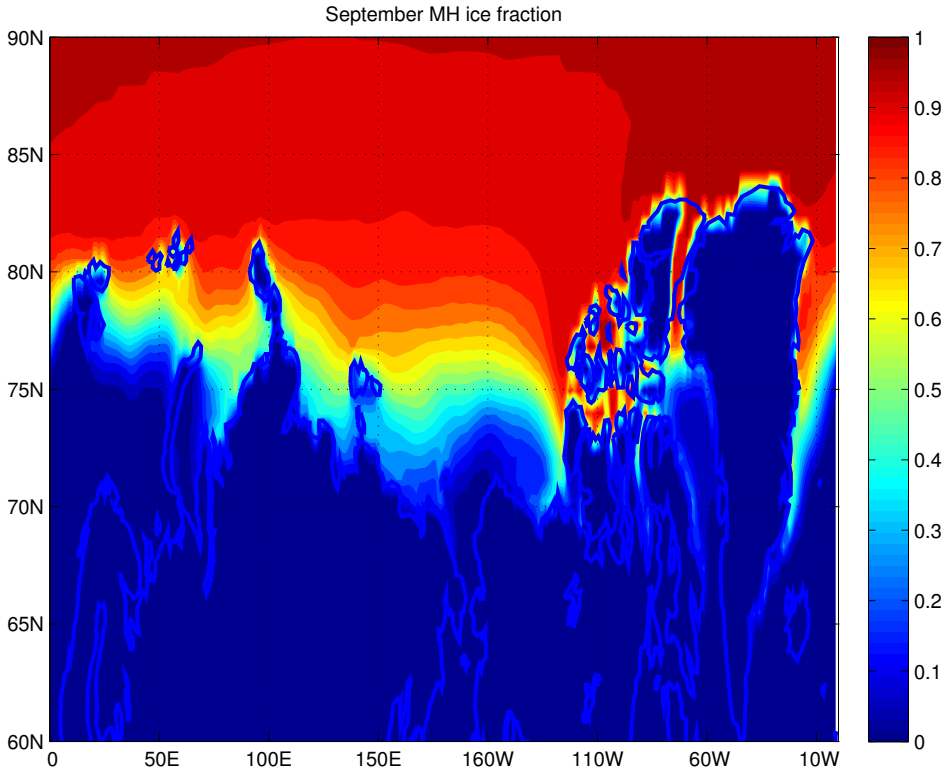

FIGURE A. 2. CCSM4 - Mid-Holocene September mean sea ice concentration

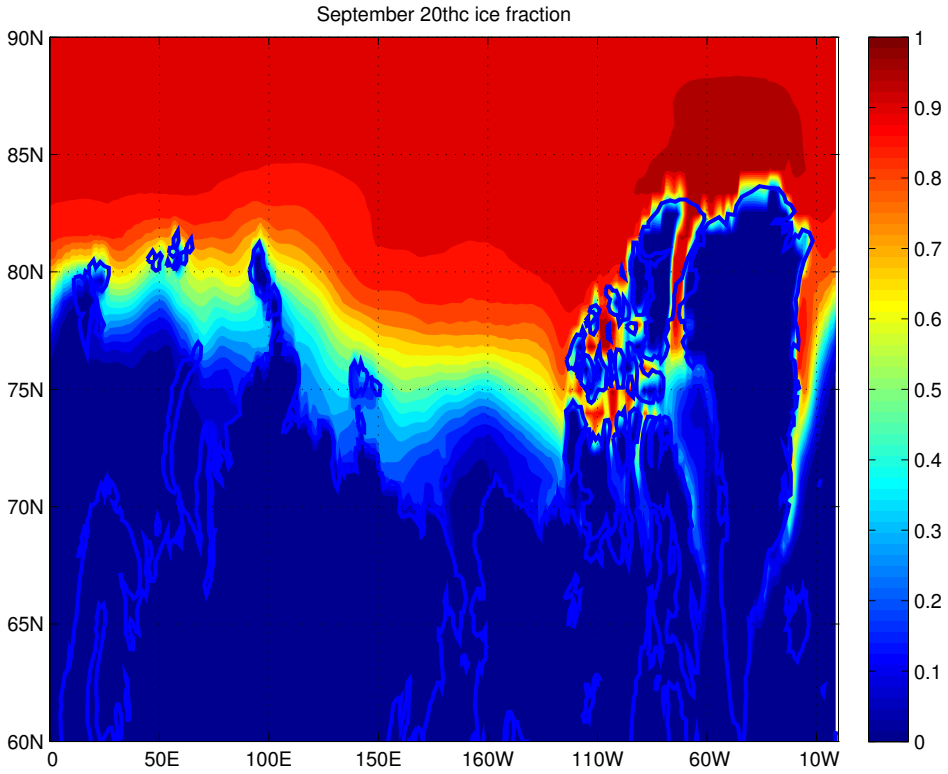

FIGURE A. 3. CCSM4 - 20th Century September mean sea ice concentration

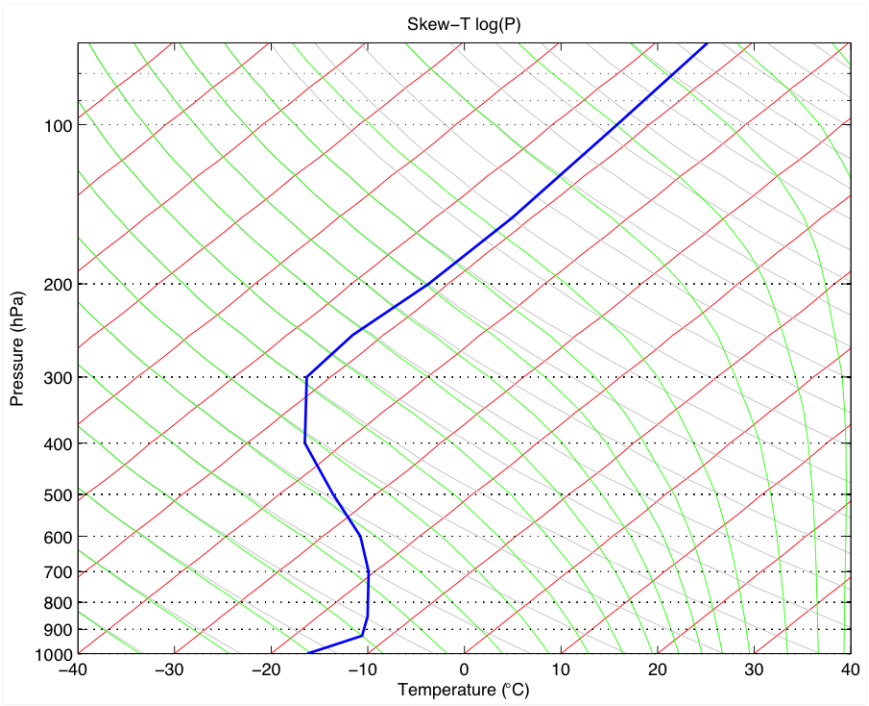

FIGURE A. 4. NCEP/NCAR - North Pole Skew-T log-P

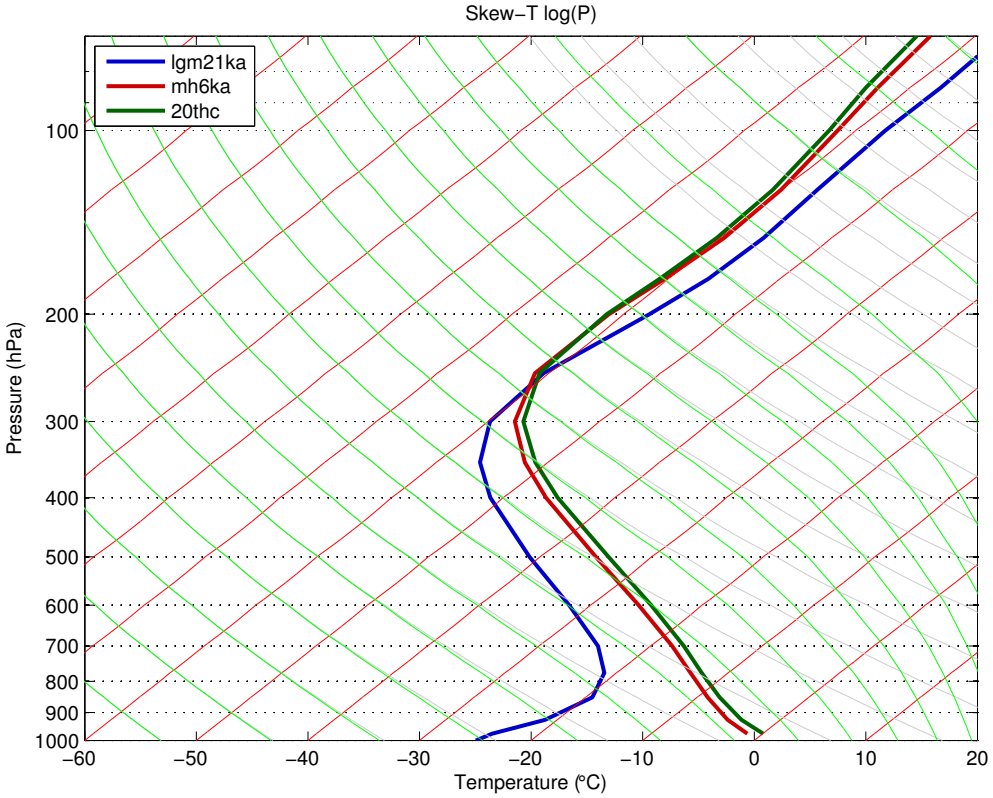

FIGURE A. 5. CCSM4 - Iceland DJF Skew-T log-P 65.5 °N 7.5 °W

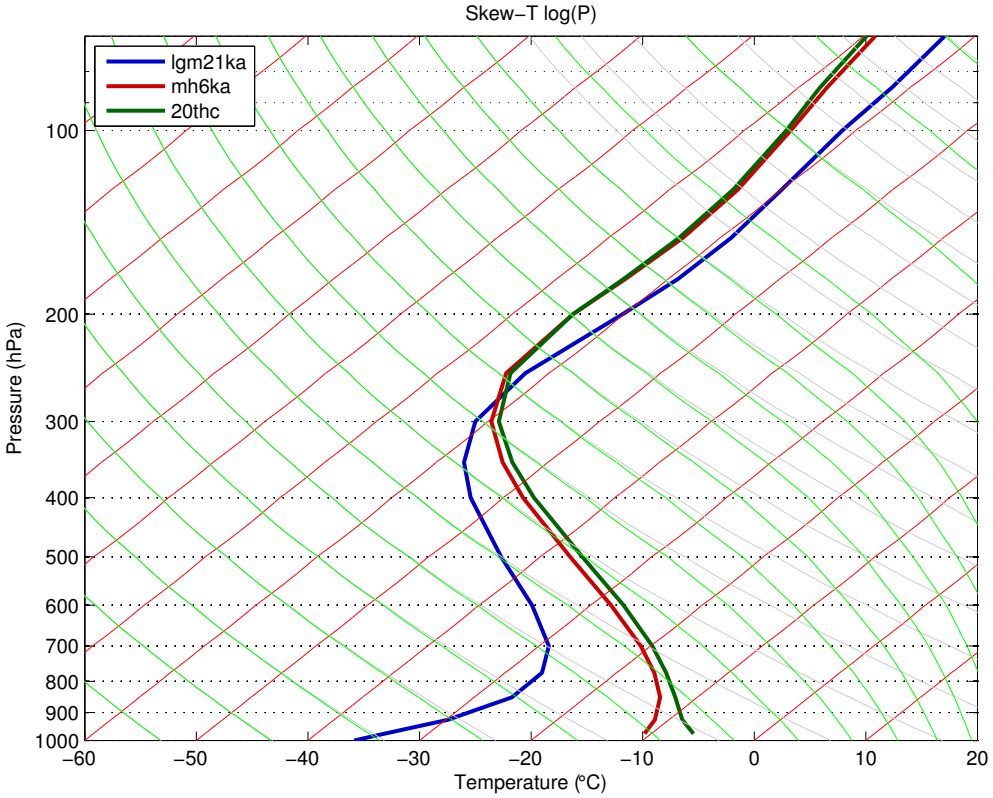

FIGURE A. 6. CCSM4 - Jan Mayen DJF Skew-T log-P 71.2 °N 7.5 °W

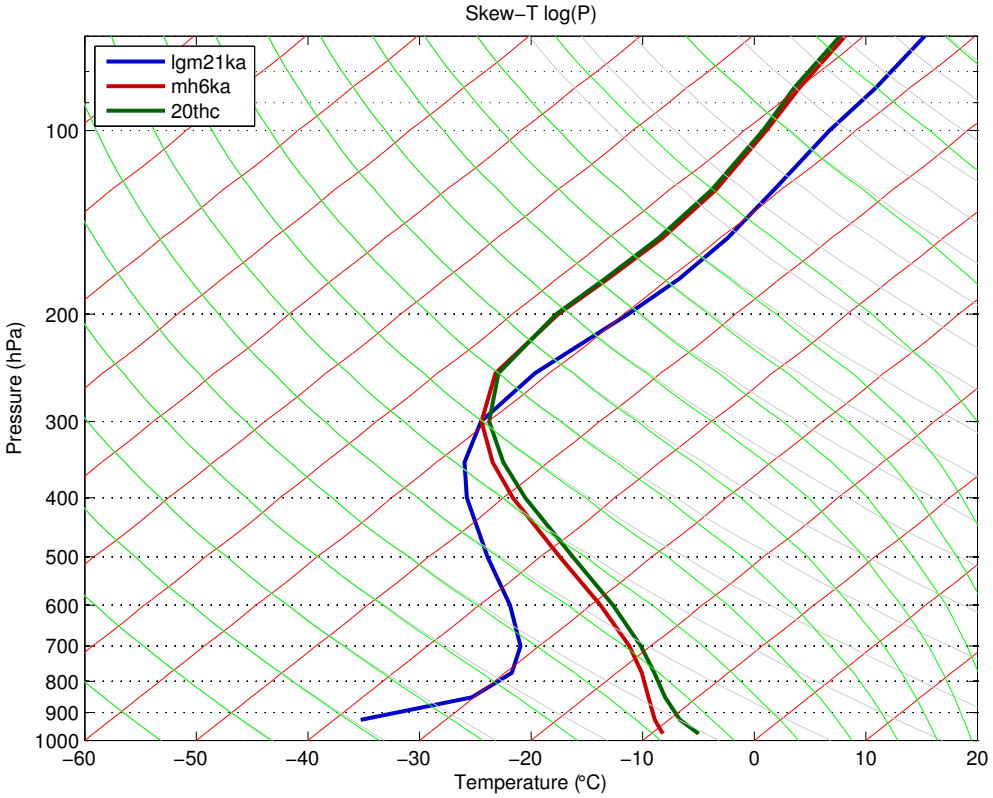

FIGURE A. 7. CCSM4 - DJF Skew-T log-P 74.9 °N 7.5 °W

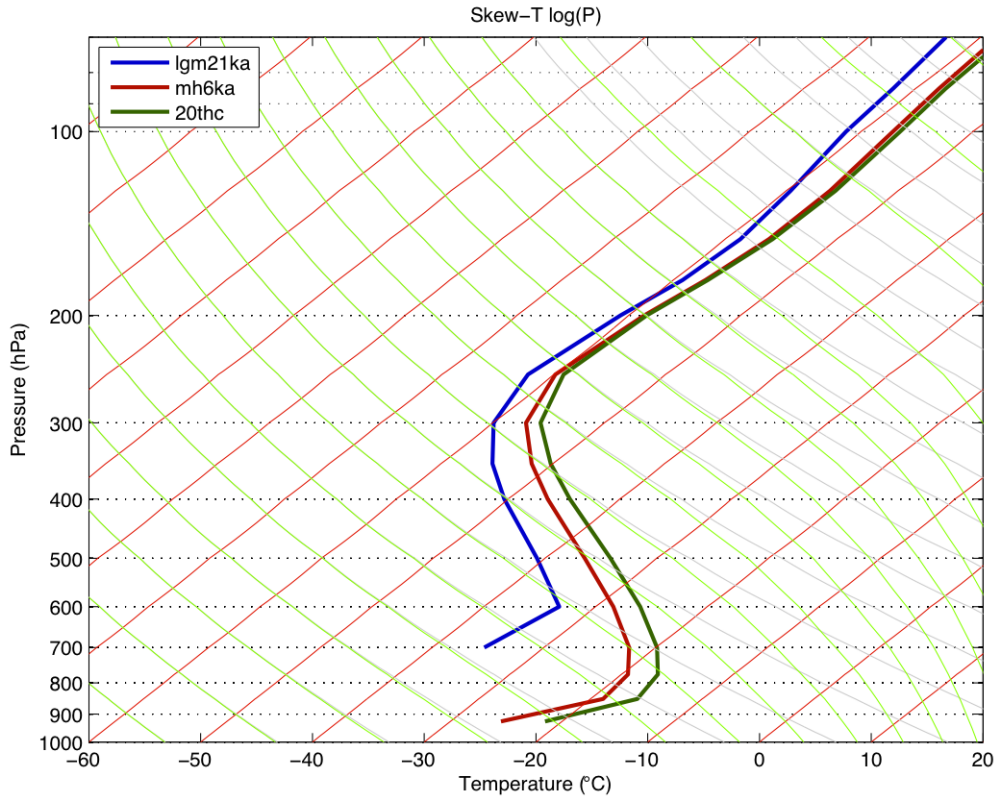

FIGURE A. 8. CCSM4 - Canadian Arctic Archipelago DJF Skew-T log-P 65 °N 110 °W

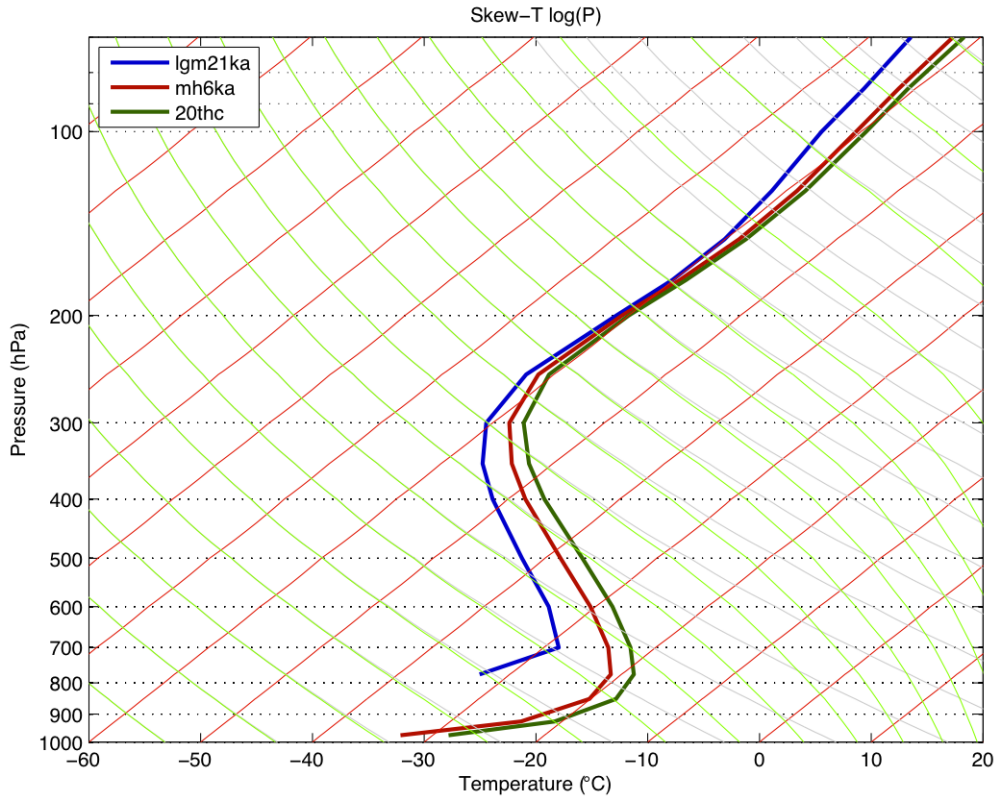

FIGURE A. 9. CCSM4 - Canadian Arctic Archipelago DJF Skew-T log-P 71 °N 110 °W

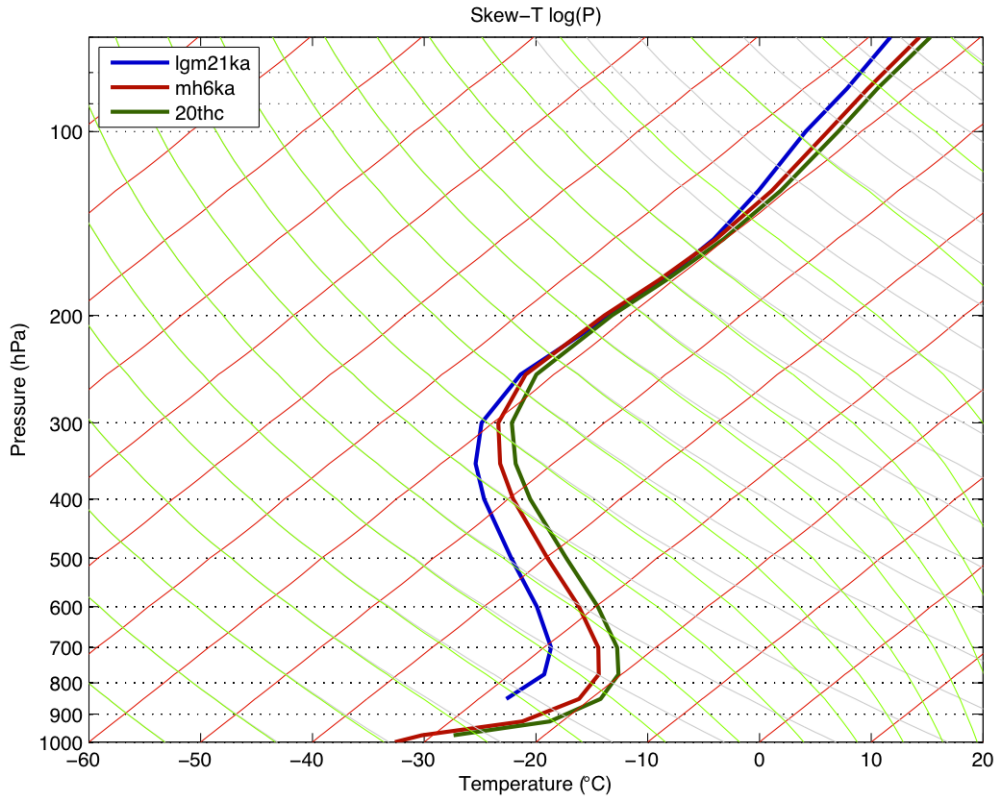

FIGURE A. 10. CCSM4 - Canadian Arctic Archipelago DJF Skew-T log-P 75 °N 110 °W

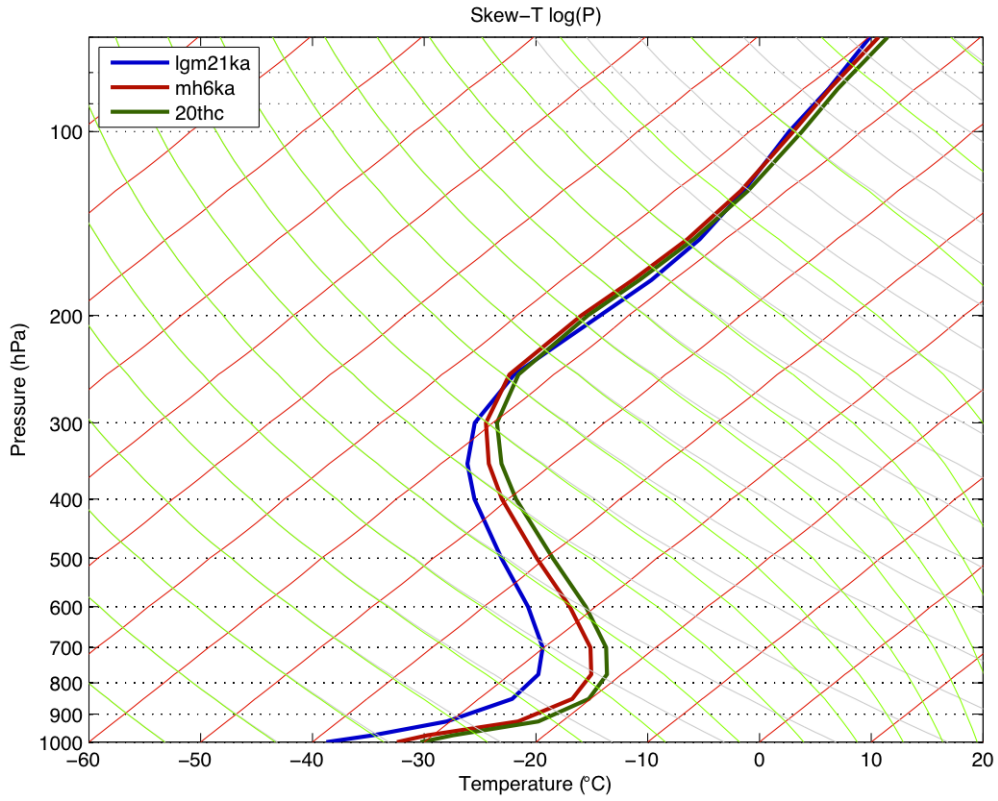

FIGURE A. 11. CCSM4 - Canadian Arctic Archipelago DJF Skew-T log-P 80 °N 110 °W

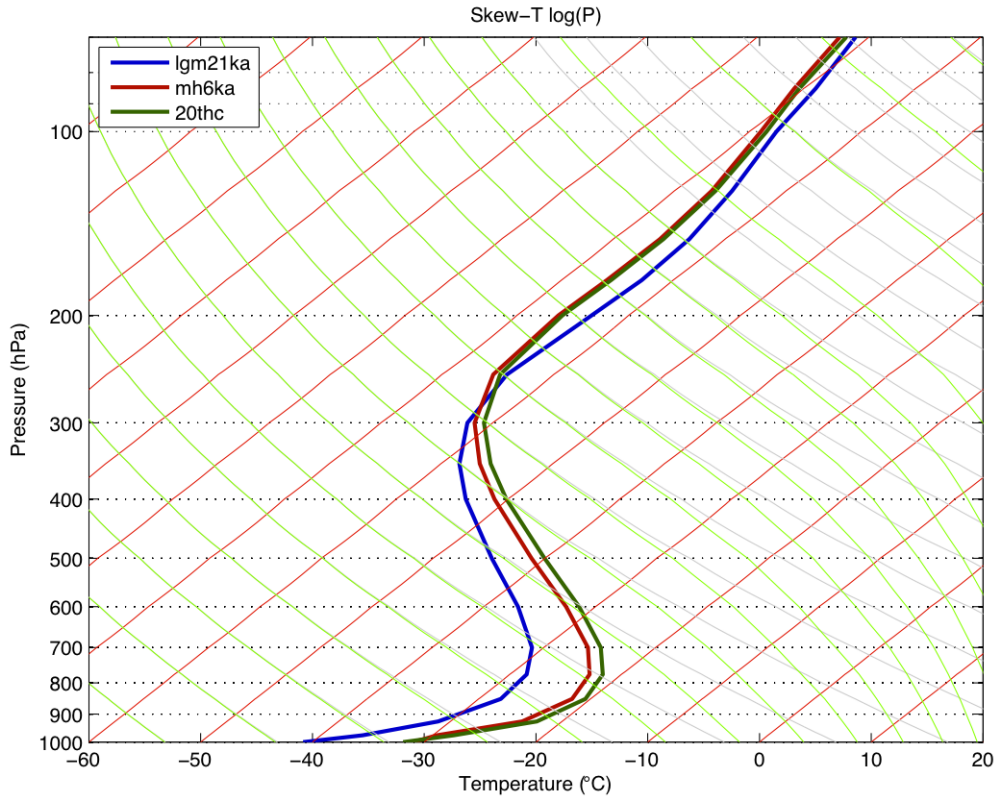

FIGURE A. 12. CCSM4 - Canadian Arctic Archipelago DJF Skew-T log-P 85 °N 110 °W

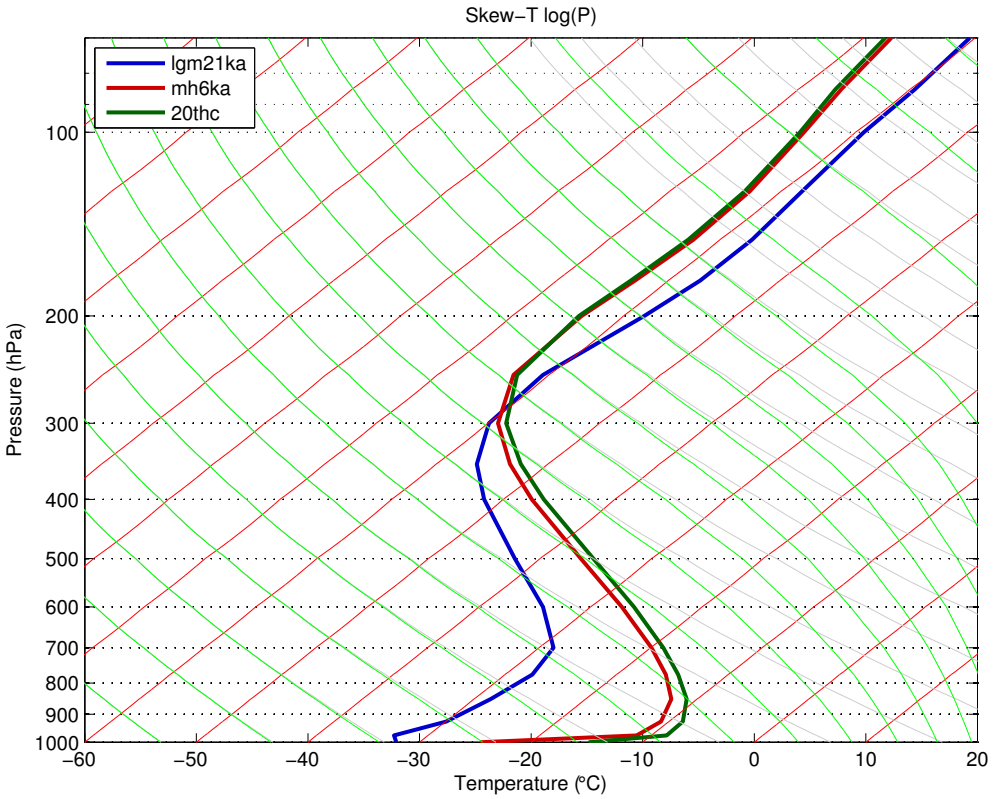

FIGURE A. 13. CCSM4 - Mean North Atlantic Storm Track (60 °N-80 °N/0 °E-50 °E) DJF Skew-T log-P

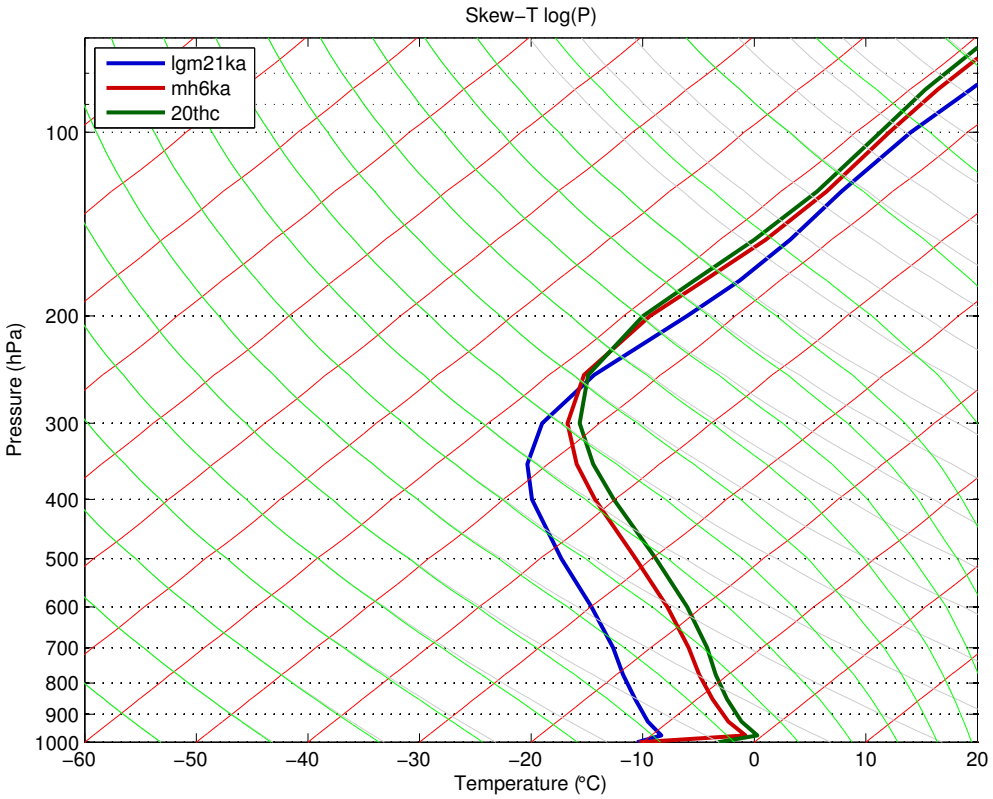

FIGURE A. 14. CCSM4 - Mean North American coast (50 °N-60 °N/60 °W-10 °W) DJF Skew-T log-P

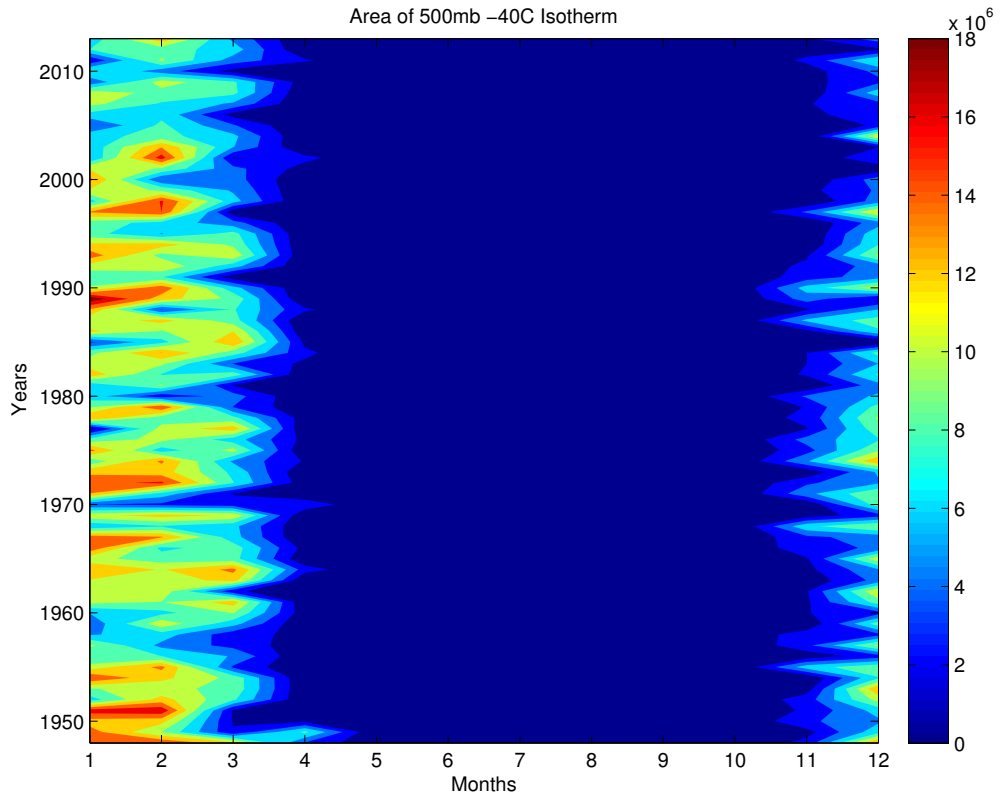

FIGURE A. 15. NCEP - Satellite era Arctic area where 500 hPa temperatures $<-40\,^{\circ}\mathrm{C}$ in km^2

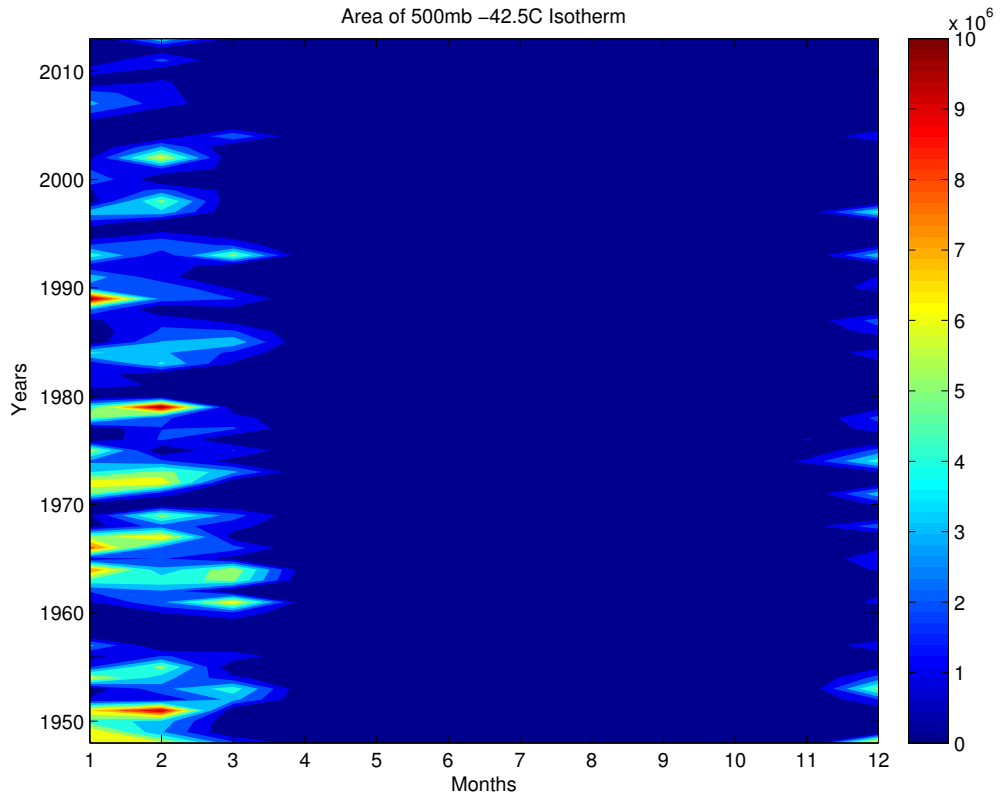

FIGURE A. 16. NCEP - Satellite era Arctic area where 500 hPa temperatures $<-42.5\,^{\circ}\mathrm{C}$ in km^2

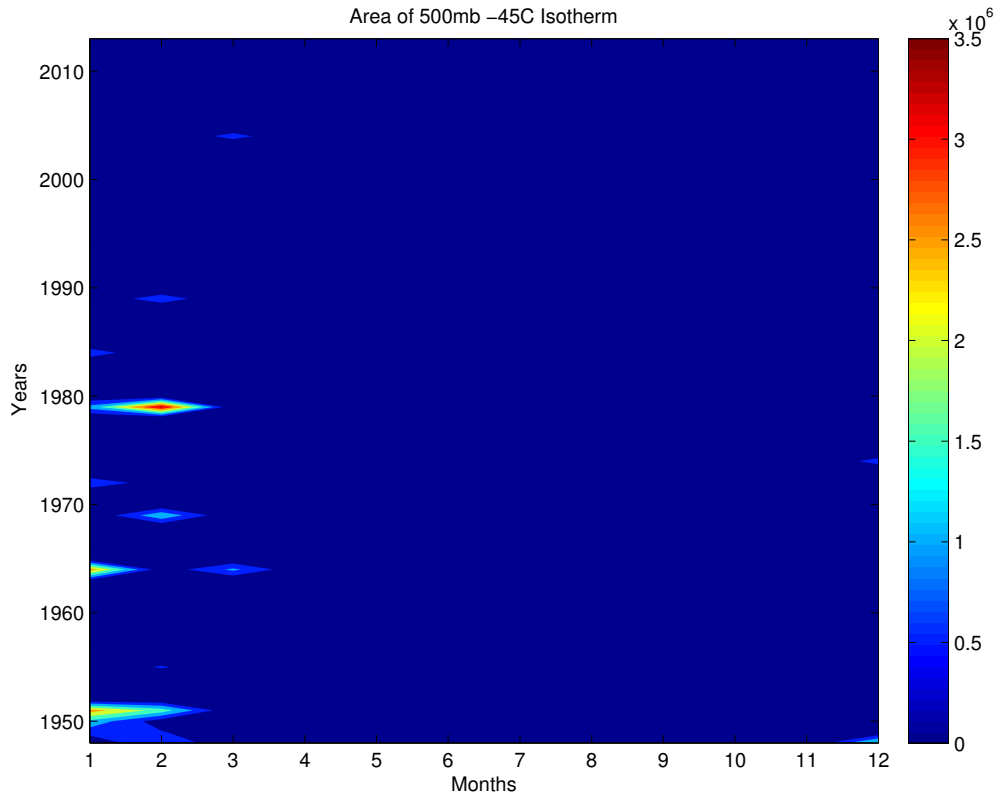

FIGURE A. 17. NCEP - Satellite era Arctic area where 500 hPa temperatures $<-45\,^{\circ}\mathrm{C}$ in km^2

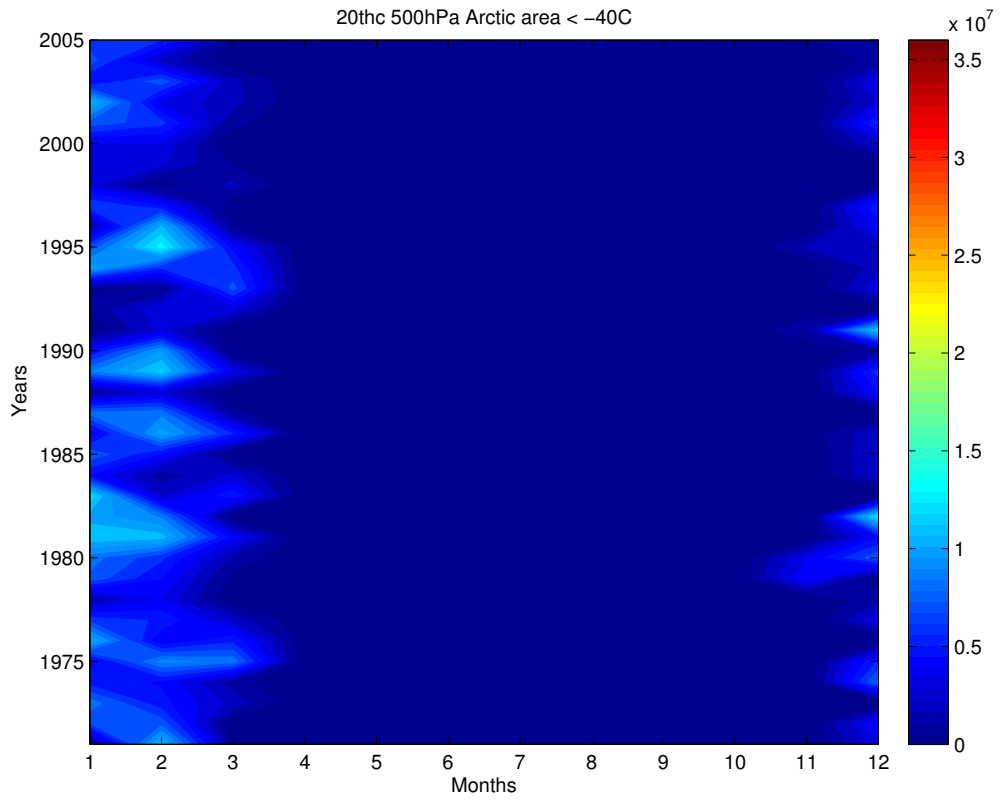

FIGURE A. 18. CCSM4 - 20thc Arctic area where 500 hPa temperatures $<-40\,^{\circ}\mathrm{C}$ in km^2

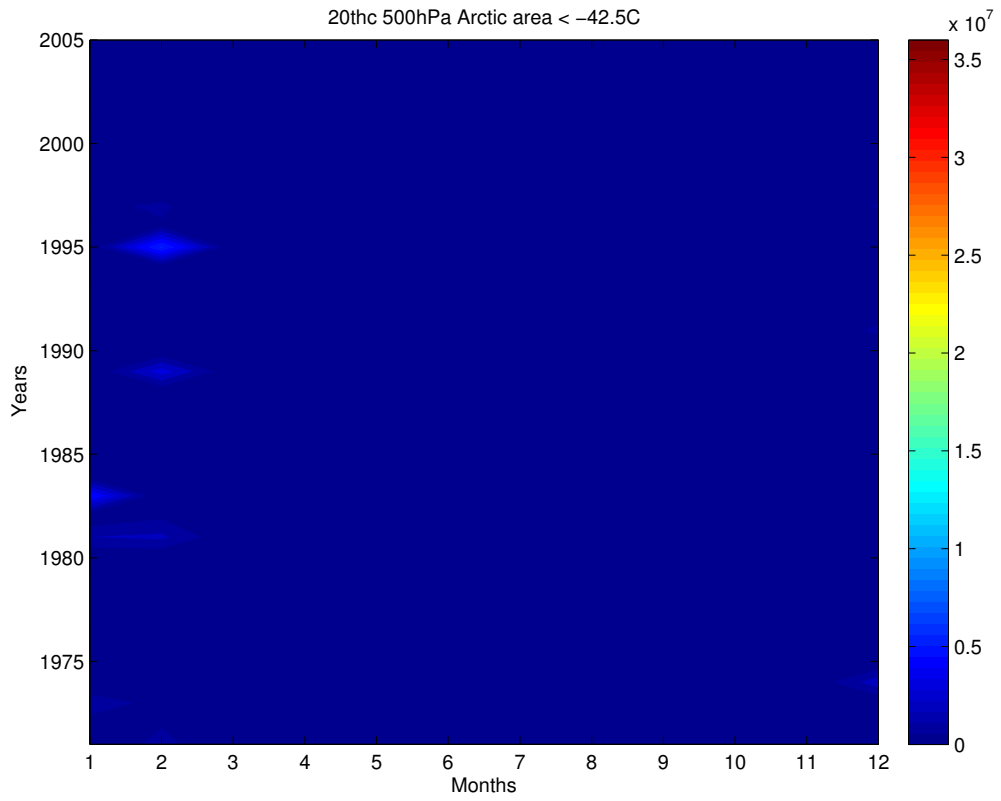

FIGURE A. 19. CCSM4 - 20thc Arctic area where 500 hPa temperatures $<-42.5\,^{\circ}\mathrm{C}$ in km^2

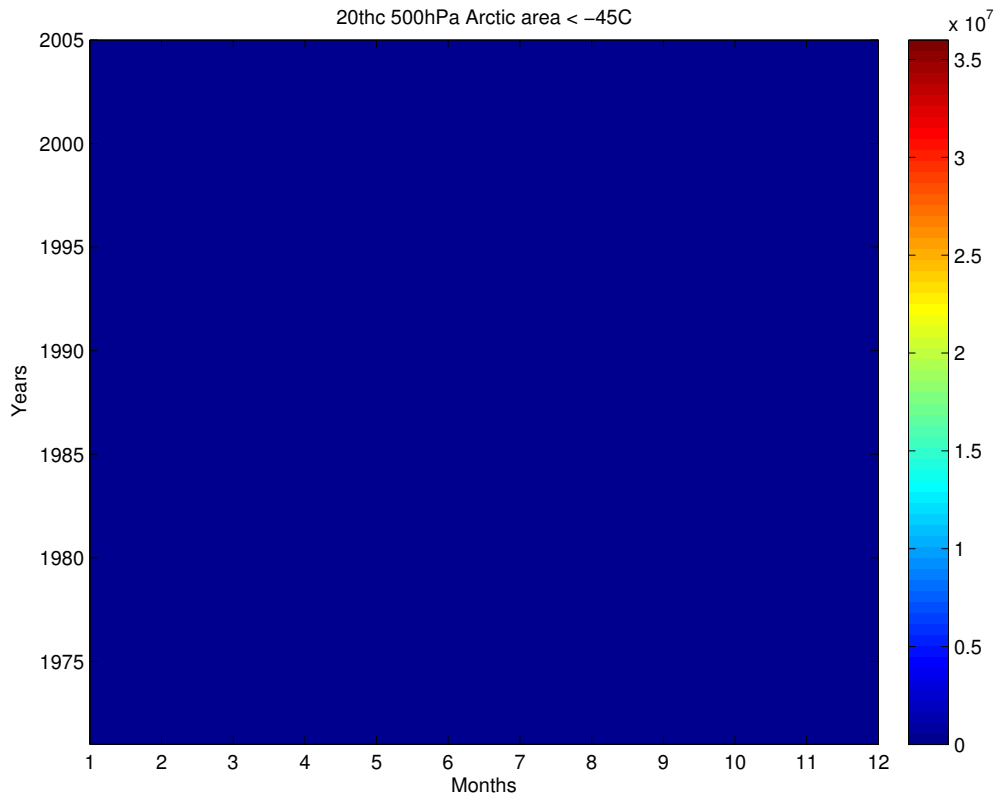

FIGURE A. 20. CCSM4 - 20thc Arctic area where 500 hPa temperatures $<-45\,^{\circ}\mathrm{C}$ in km^2

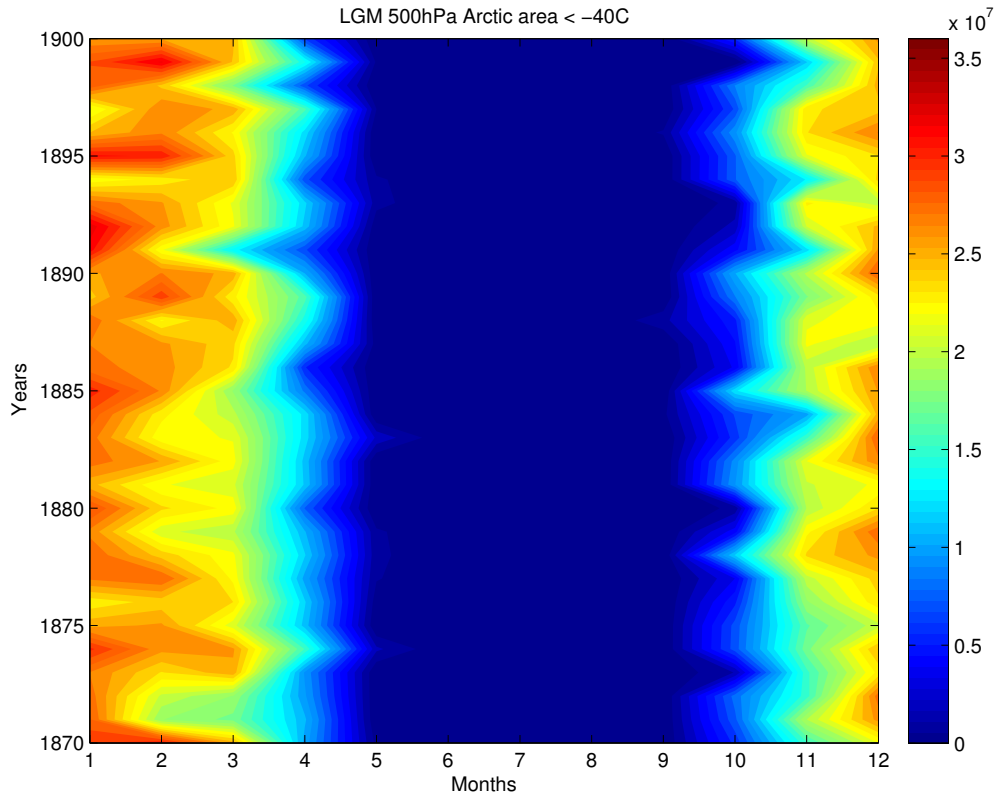

FIGURE A. 21. CCSM4 - Last Glacial Maximum Arctic area where 500 hPa temperatures $<-40\,^{\circ}\mathrm{C}$ in km^2

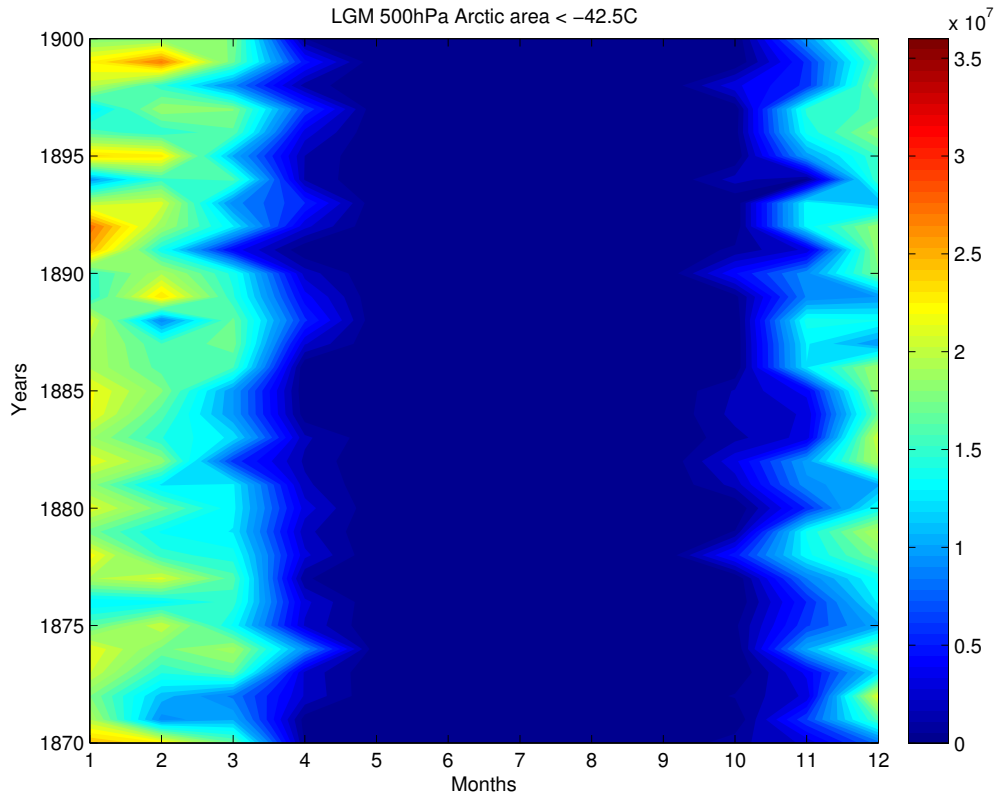

FIGURE A. 22. CCSM4 - Last Glacial Maximum Arctic area where 500 hPa temperatures $<-42.5\,^{\circ}\mathrm{C}$ in km^2

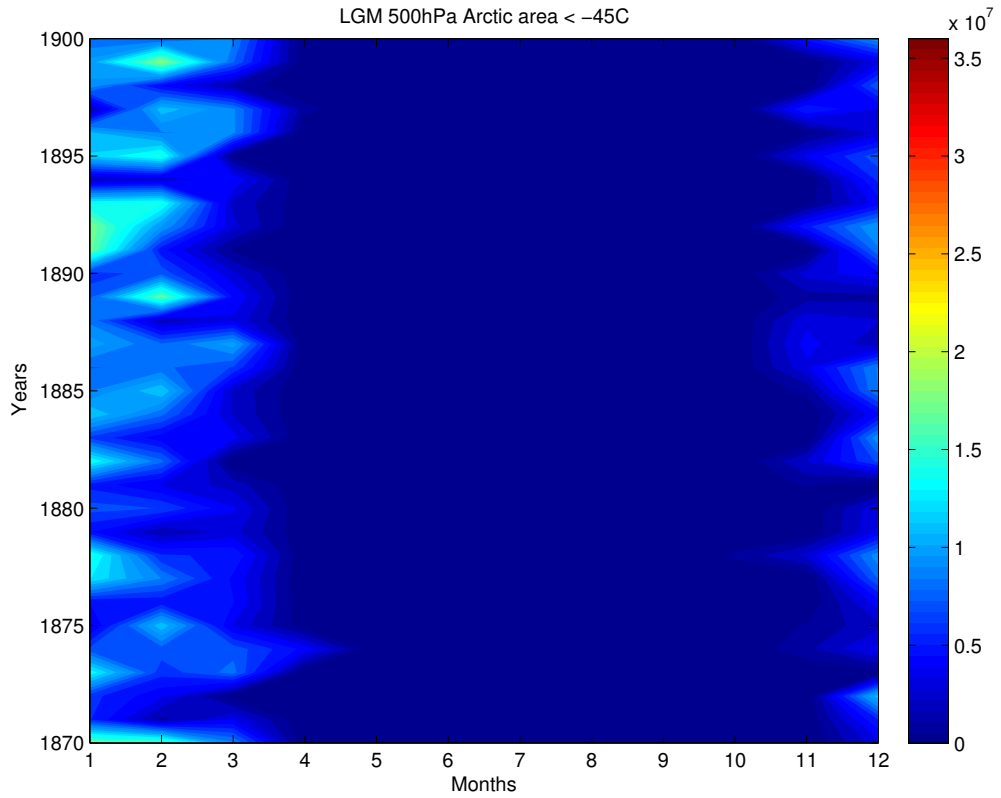

FIGURE A. 23. CCSM4 - Last Glacial Maximum Arctic area where 500 hPa temperatures $<-45\,^{\circ}\mathrm{C}$ in km^2

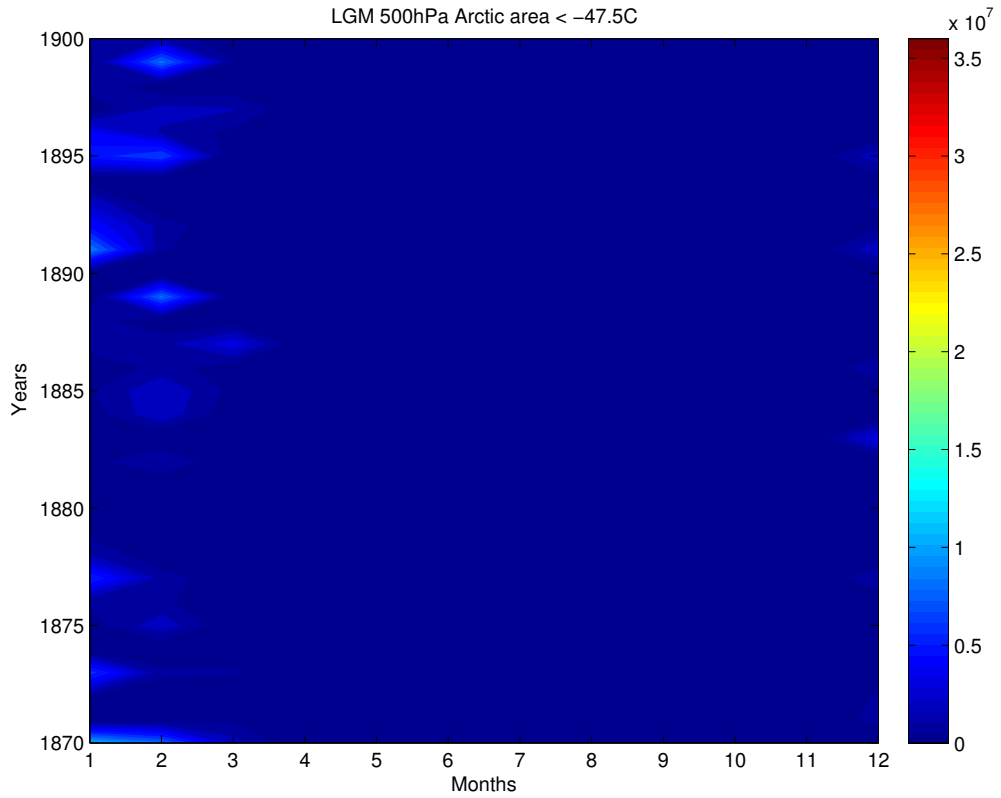

FIGURE A. 24. CCSM4 - Last Glacial Maximum Arctic area where 500 hPa temperatures $<-47.5\,^{\circ}\mathrm{C}$ in km^2

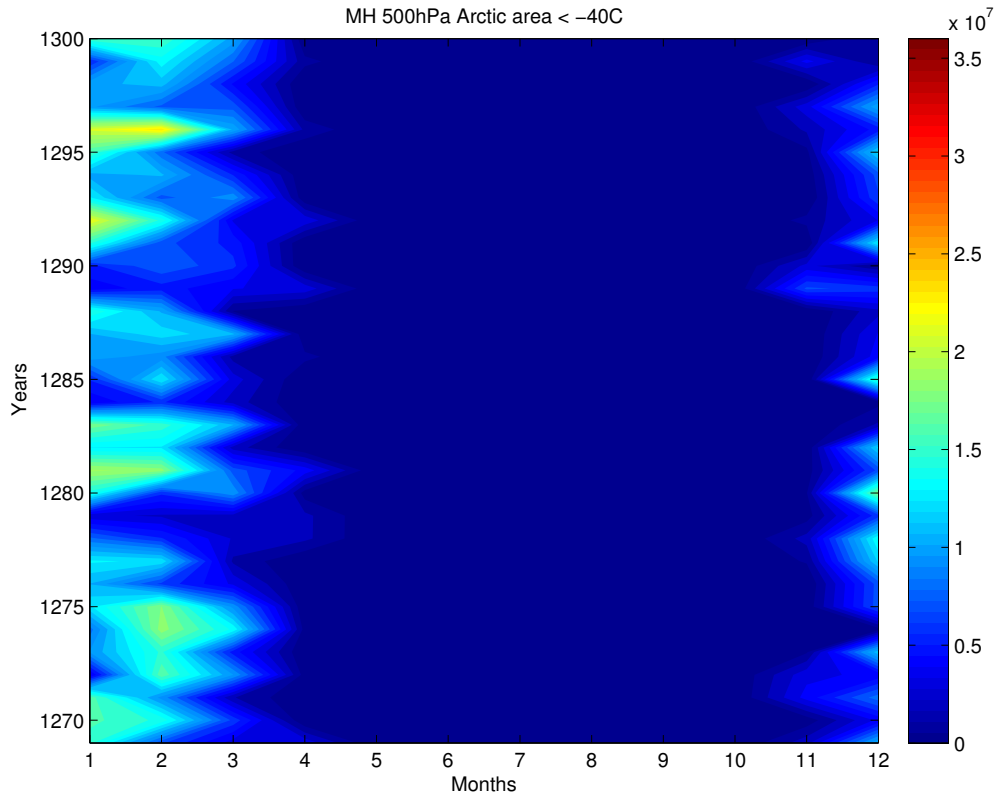

FIGURE A. 25. CCSM4 - Mid-Holocene Arctic area where 500 hPa temperatures $<-40\,^{\circ}\mathrm{C}$ in km^2

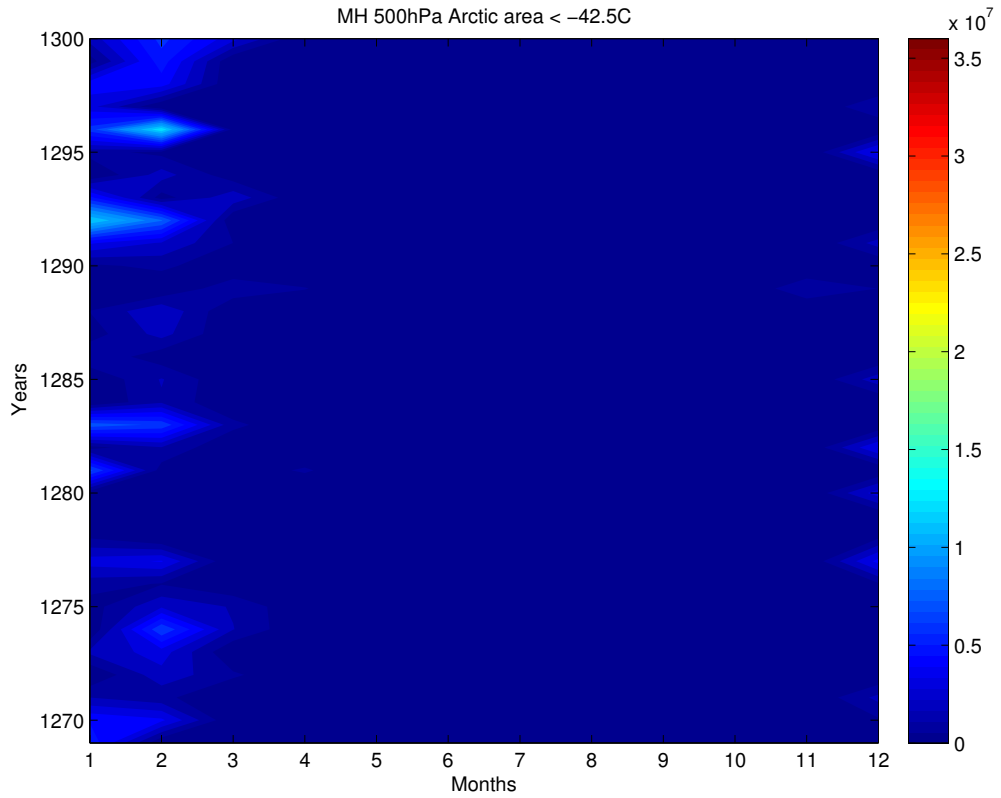

FIGURE A. 26. CCSM4 - Mid-Holocene Arctic area where 500 hPa temperatures $<-42.5\,^{\circ}\mathrm{C}$ in km^2

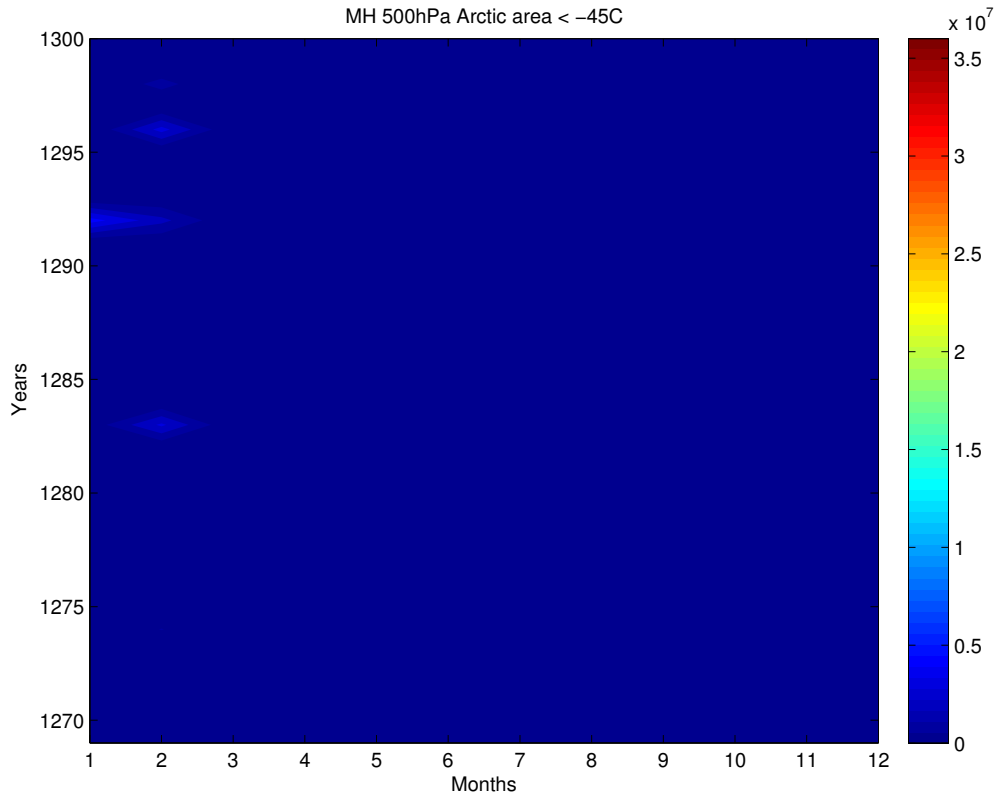

FIGURE A. 27. CCSM4 - Mid-Holocene Arctic area where 500 hPa temperatures $<-45\,^{\circ}\mathrm{C}$ in km^2

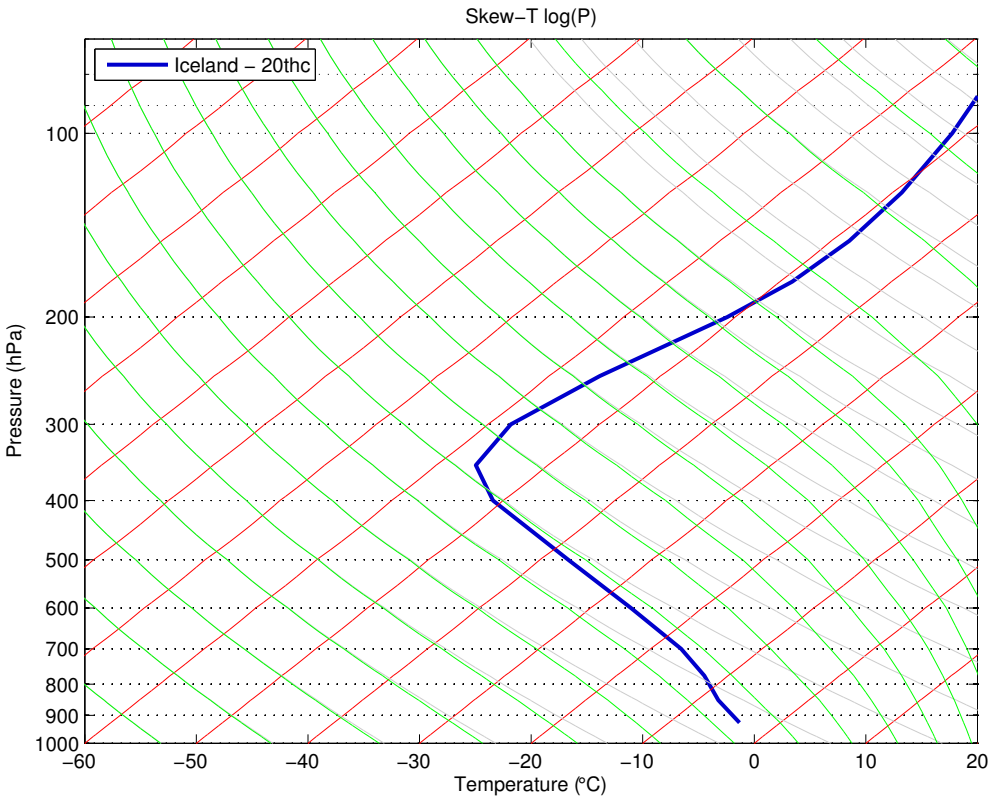

FIGURE A. 28. CCSM4 - Moist adiabatic temperature profile where P* 0 over Iceland

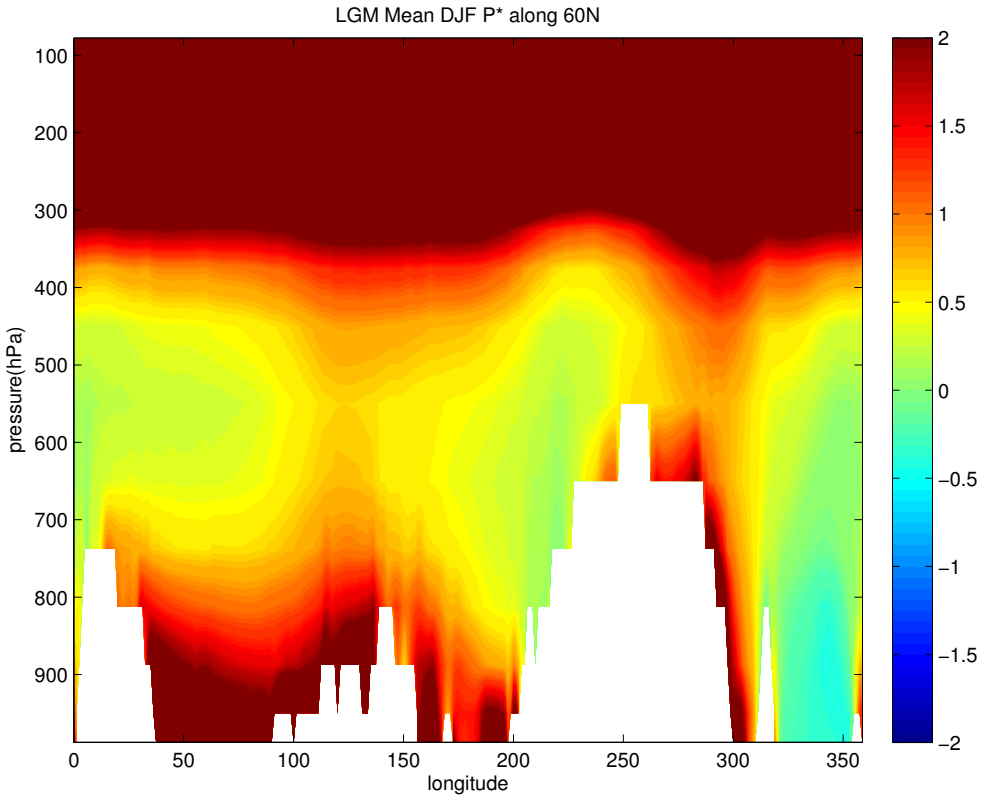

FIGURE A. 29. CCSM4 - Last glacial maximum P* cross section taken at 60 °N in PVU

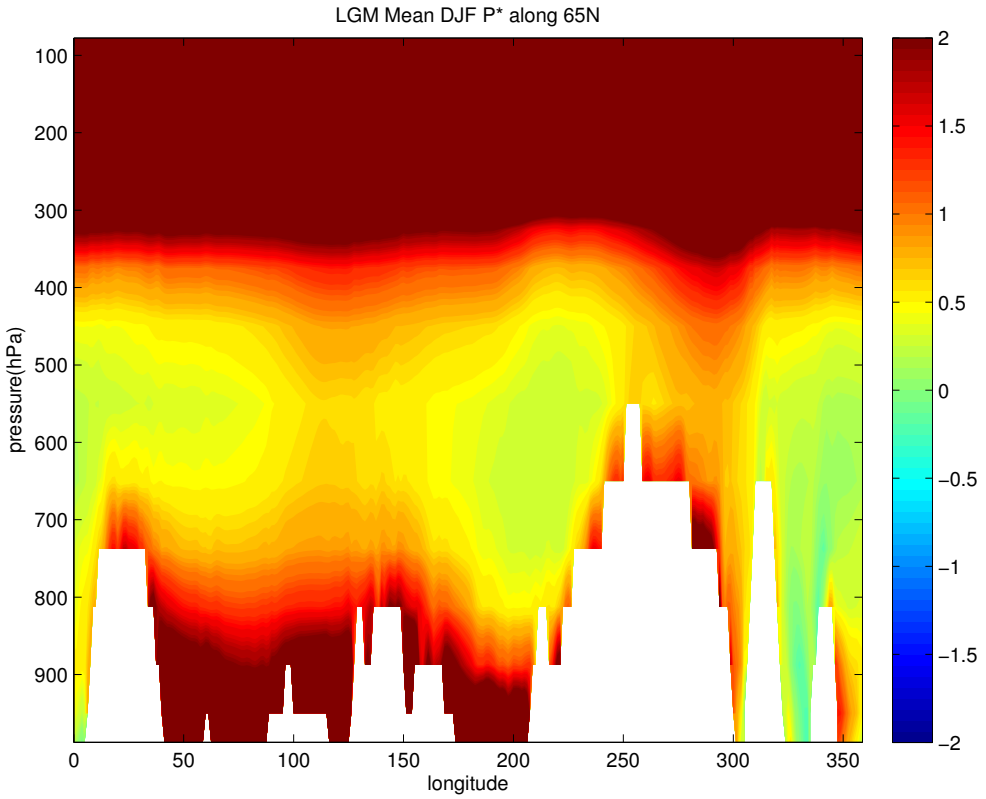

FIGURE A. 30. CCSM4 - Last glacial maximum P* cross section taken at 65 °N in PVU

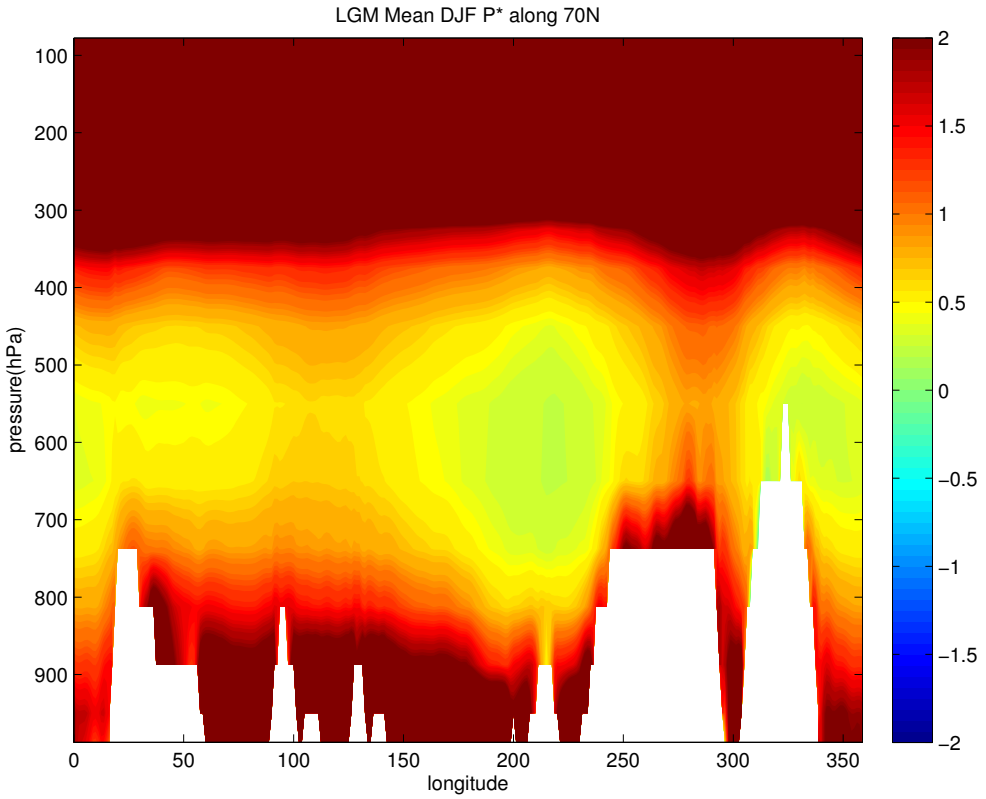

FIGURE A. 31. CCSM4 - Last glacial maximum P* cross section taken at 70 °N in PVU

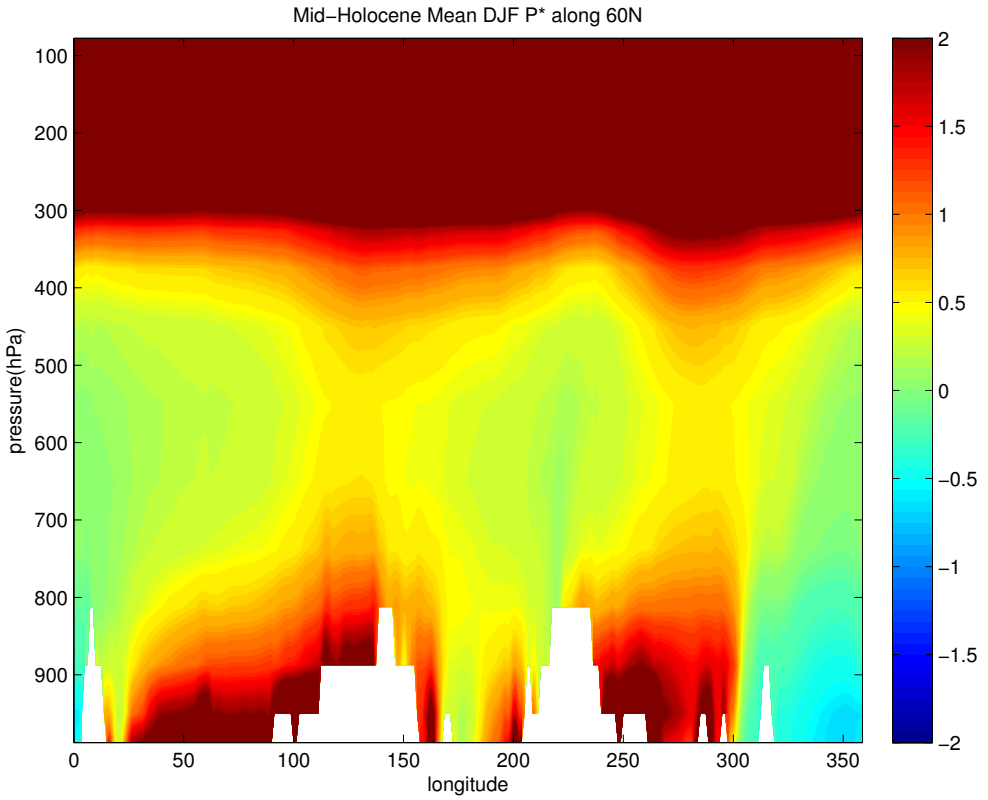

FIGURE A. 32. CCSM4 - Mid-Holocene P* cross section taken at 60 °N in PVU

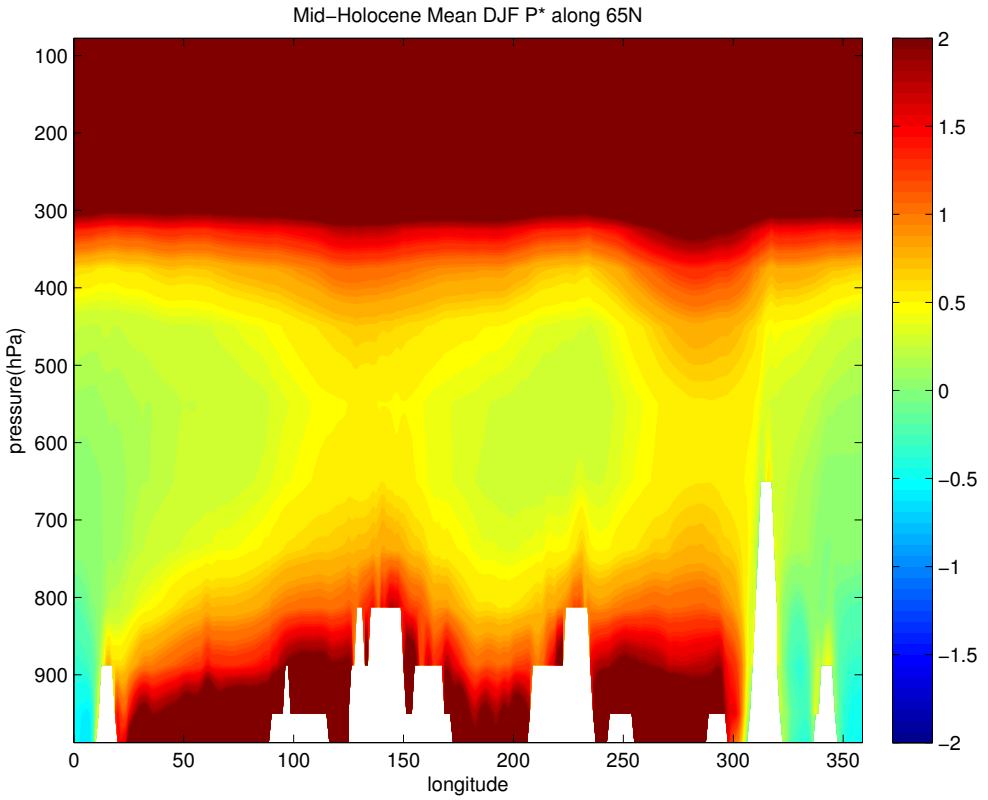

FIGURE A. 33. CCSM4 - Mid-Holocene P* cross section taken at 65 °N in PVU

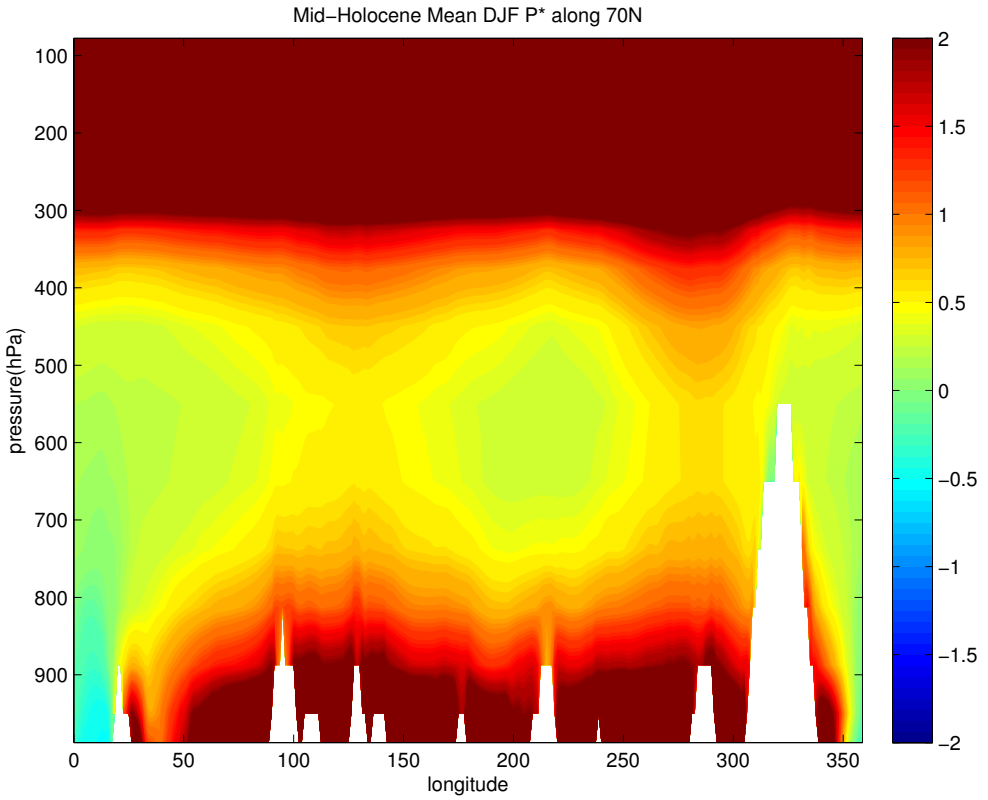

FIGURE A. 34. CCSM4 - Mid-Holocene P* cross section taken at 70 °N in PVU

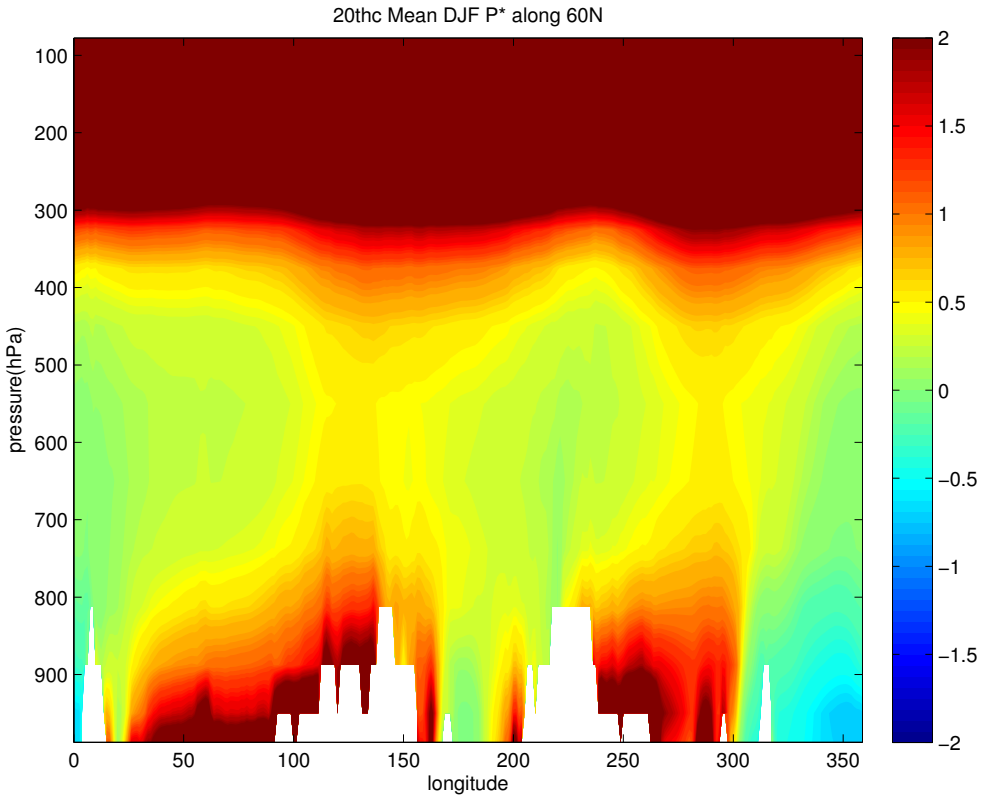

FIGURE A. 35. CCSM4 - 20th Century maximum P* cross section taken at 60 °N in PVU

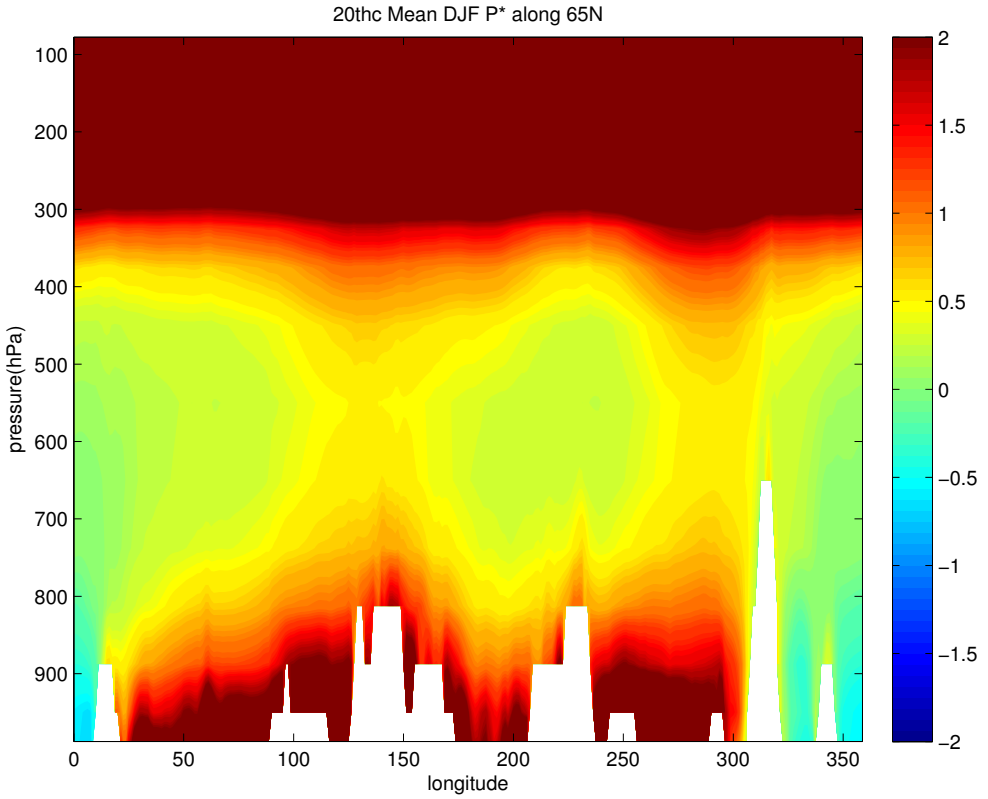

FIGURE A. 36. CCSM4 - 20th Century P* cross section taken at 65 °N in PVU

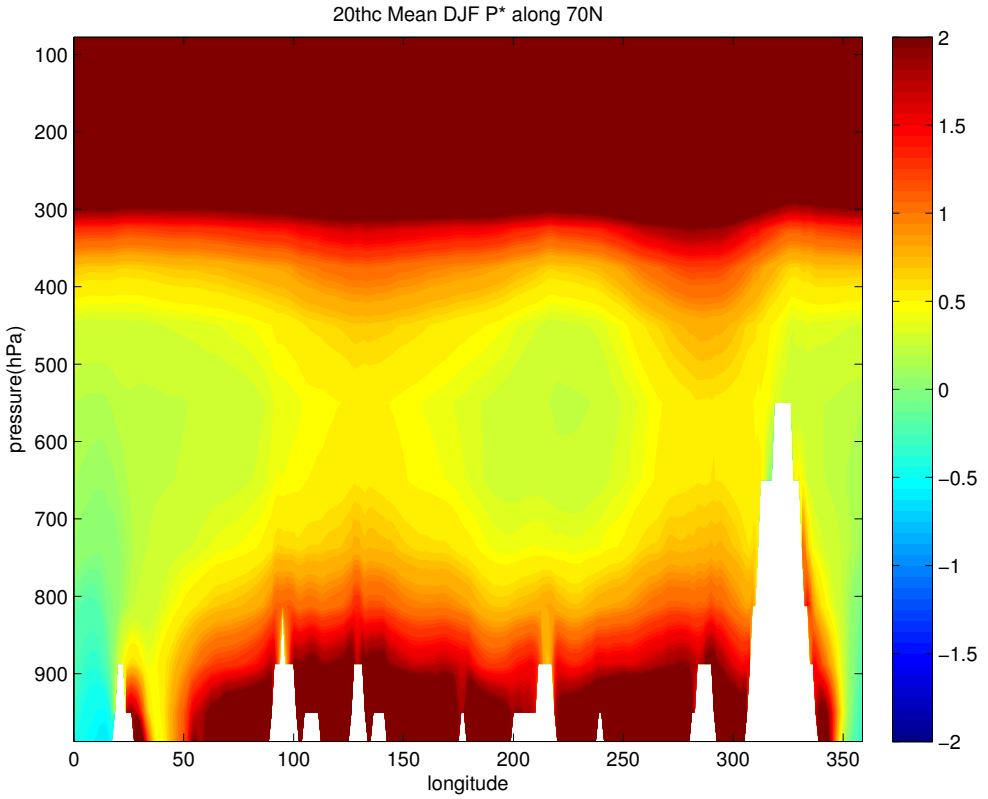

FIGURE A. 37. CCSM4 - 20th Century P* cross section taken at 70 °N in PVU

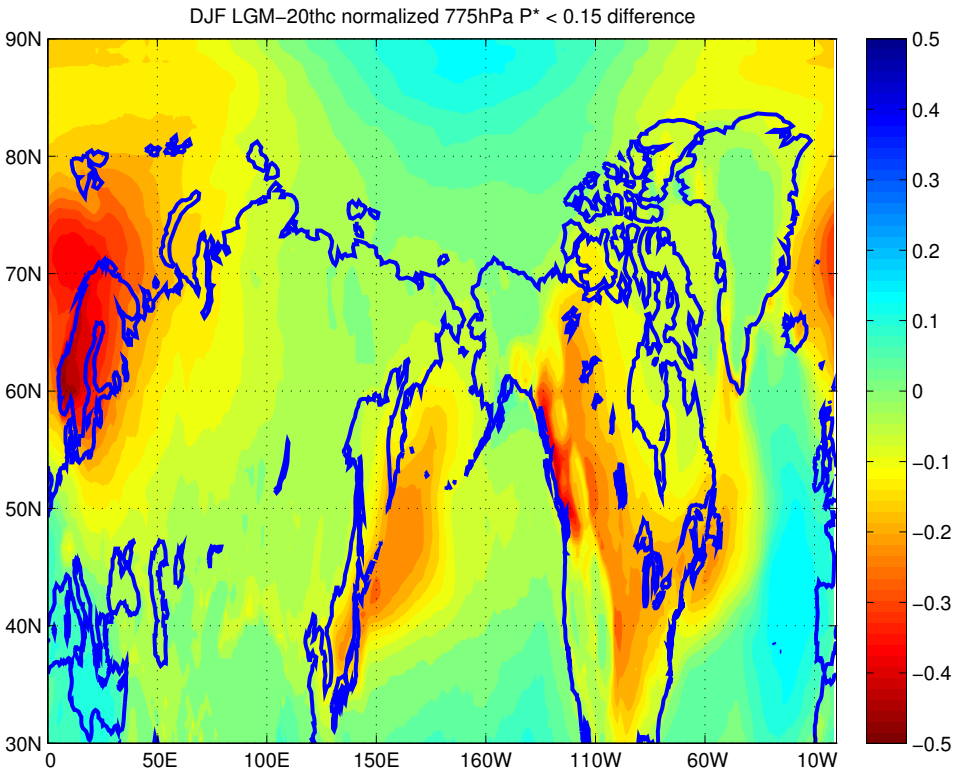

FIGURE A. 38. CCSM4 - Normalized 775 hPa DJF Last Glacial Maximum-20th Century P* <0.15 in PVU

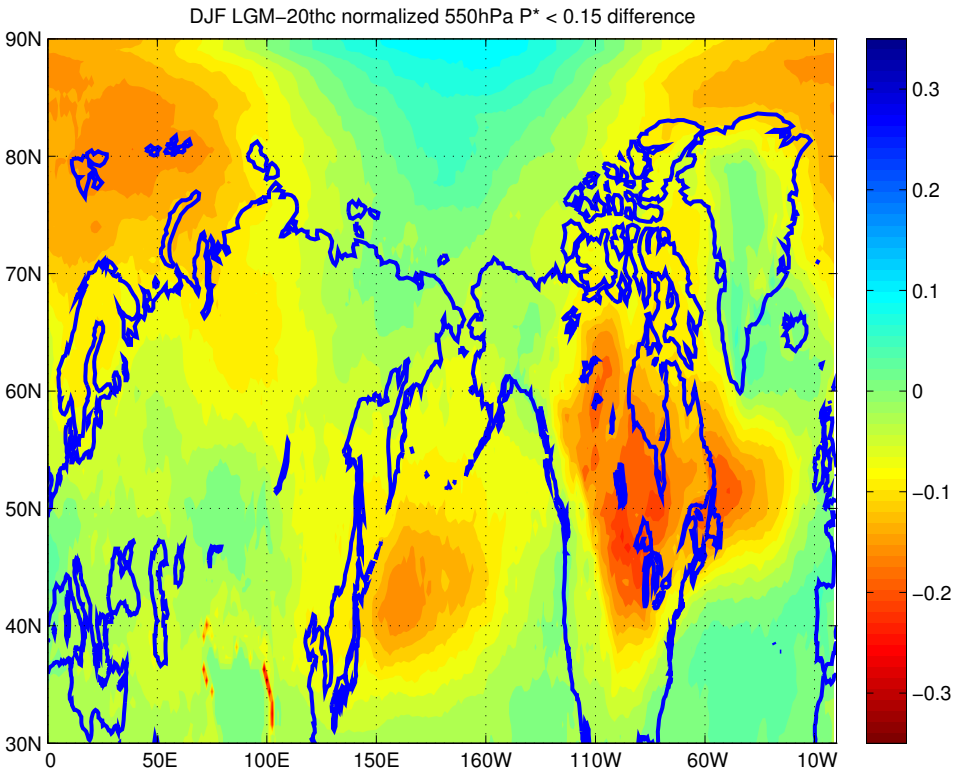

FIGURE A. 39. CCSM4 - Normalized 550 hPa DJF Last Glacial Maximum-20th Century P* <0.15 in PVU

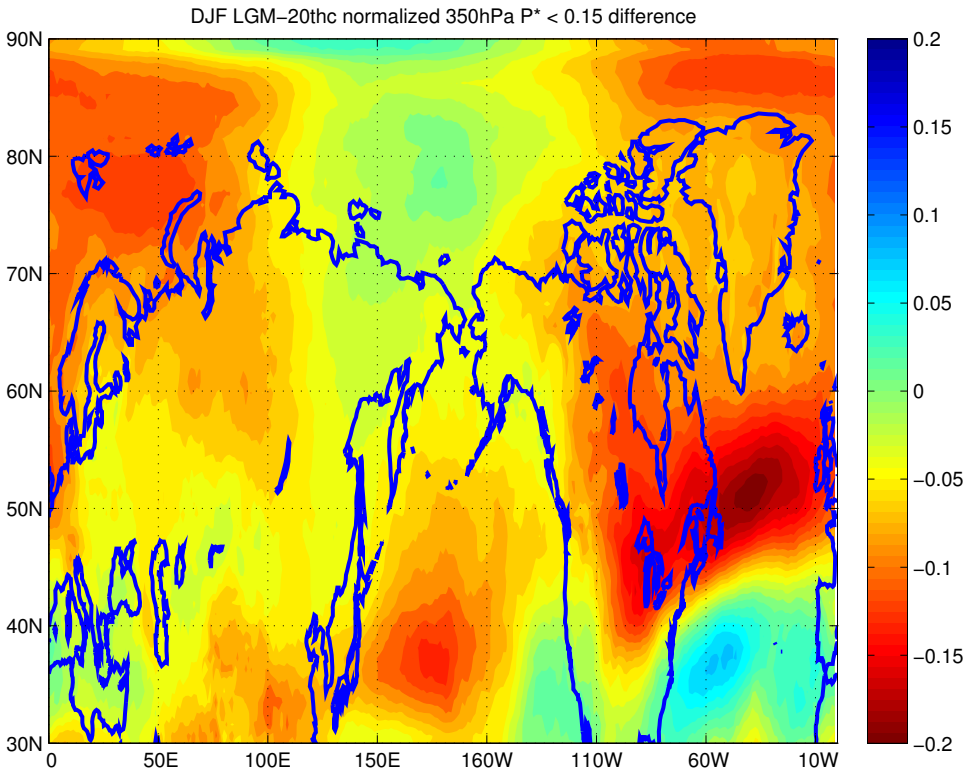

FIGURE A. 40. CCSM4 - Normalized 350 hPa DJF Last Glacial Maximum-20th Century P* <0.15 in PVU

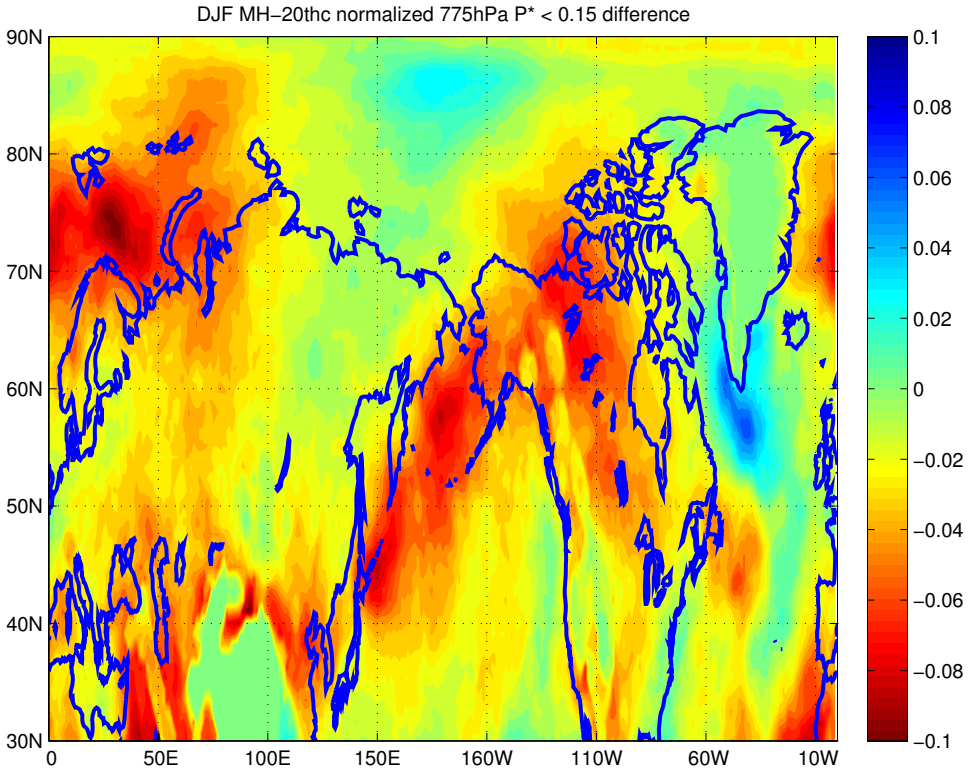

FIGURE A. 41. CCSM4 - Normalized 775 hPa DJF Mid-Holocene-20th Century P* <0.15 in PVU

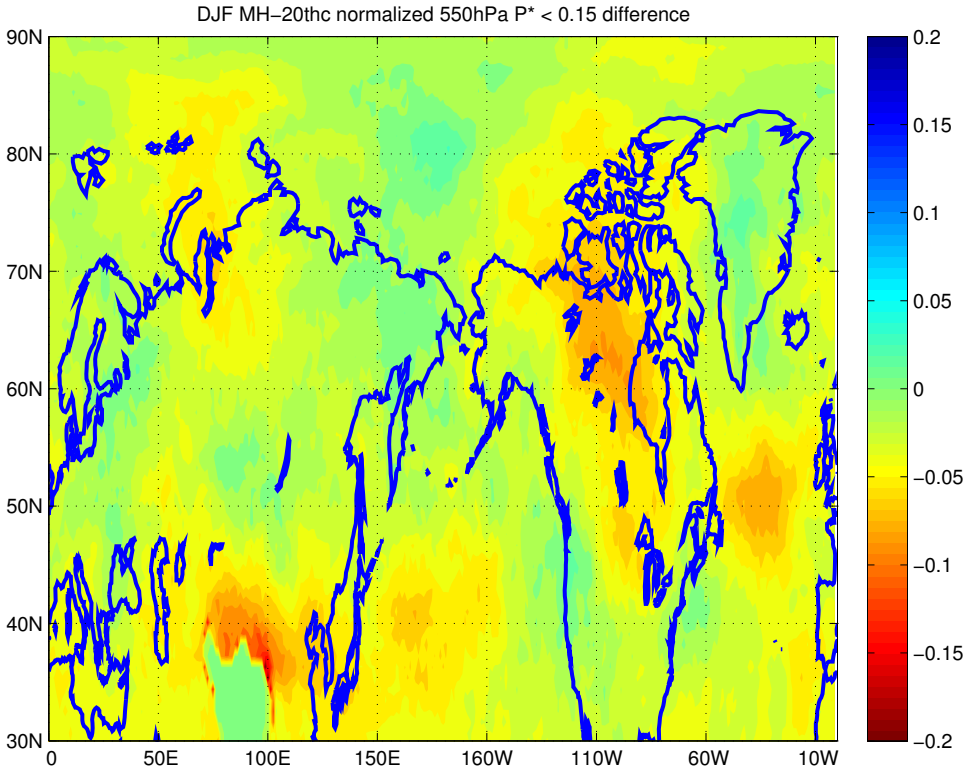

FIGURE A. 42. CCSM4 - Normalized 550 hPa DJF Mid-Holocene-20th Century P* <0.15 in PVU

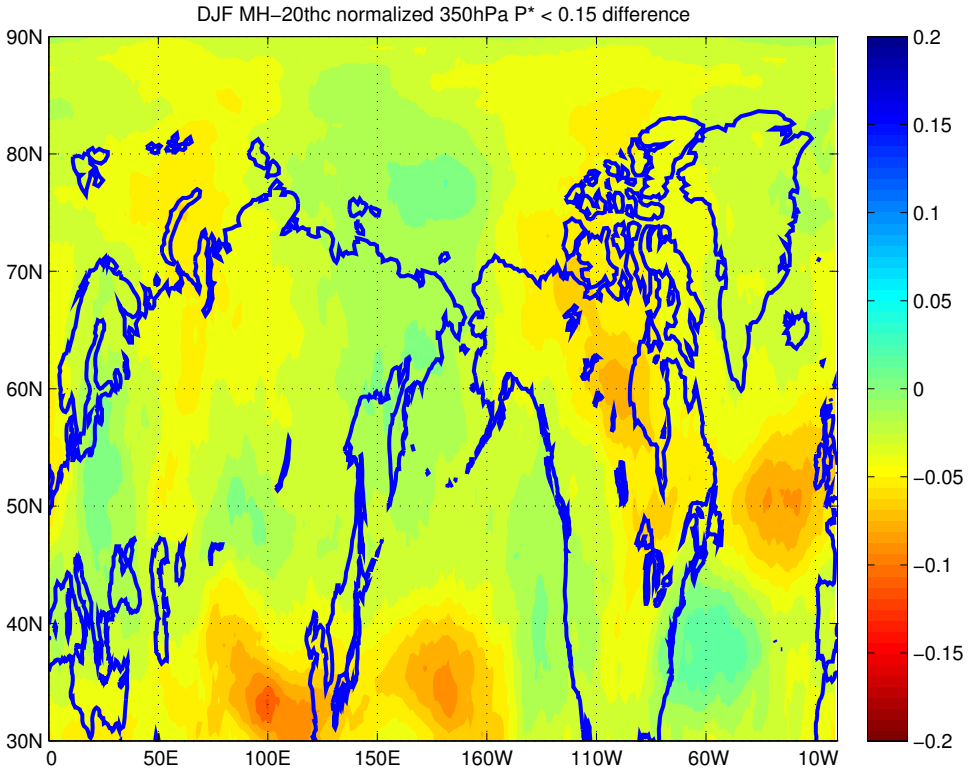

FIGURE A. 43. CCSM4 - Normalized 350 hPa DJF Mid-Holocene-20th Century P* <0.15 in PVU

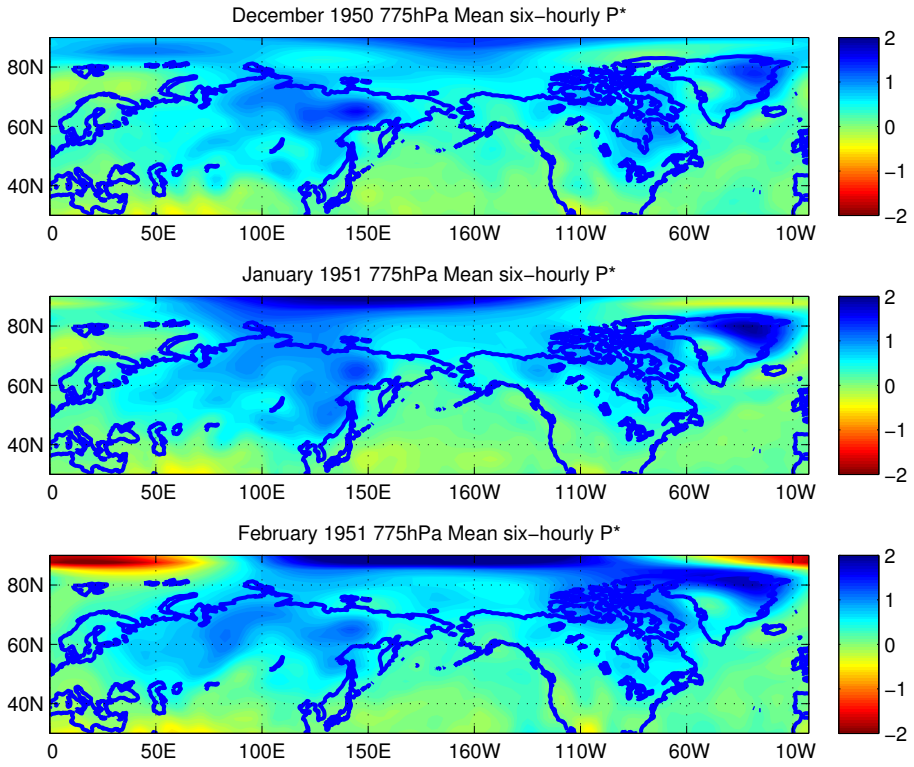

FIGURE A. 44. NCEP - 775 hPa P* from December 1950, January, and February 1951 in PVU

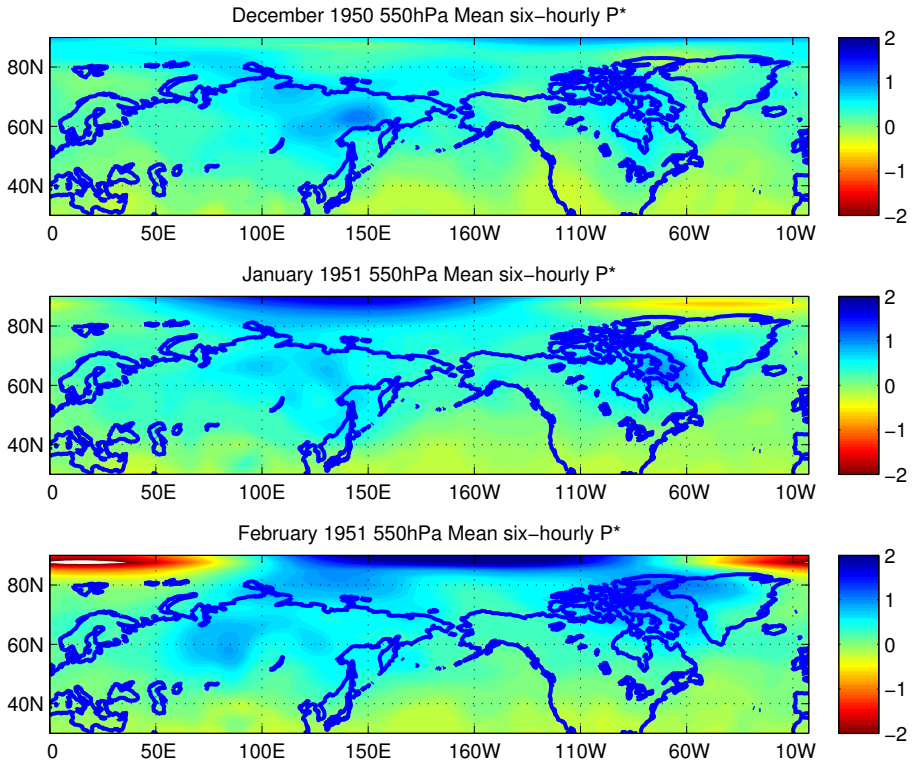

FIGURE A. 45. NCEP - 550 hPa P* from December 1950, January, and February 1951 in PVU

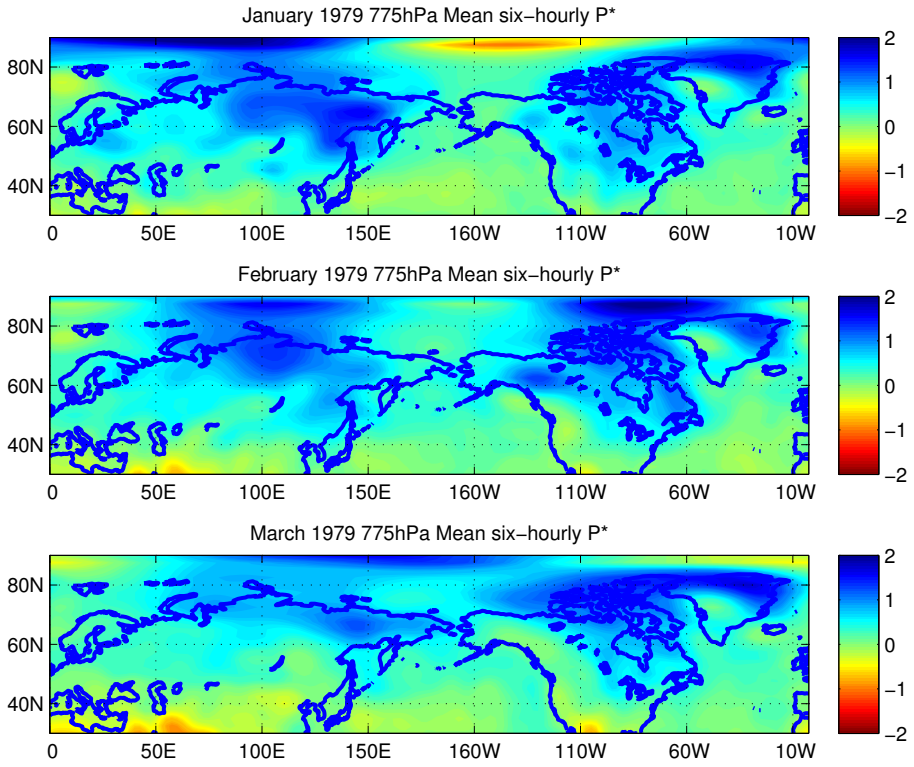

FIGURE A. 46. NCEP - 775 hPa P* from January, February, and March 1979 in PVU

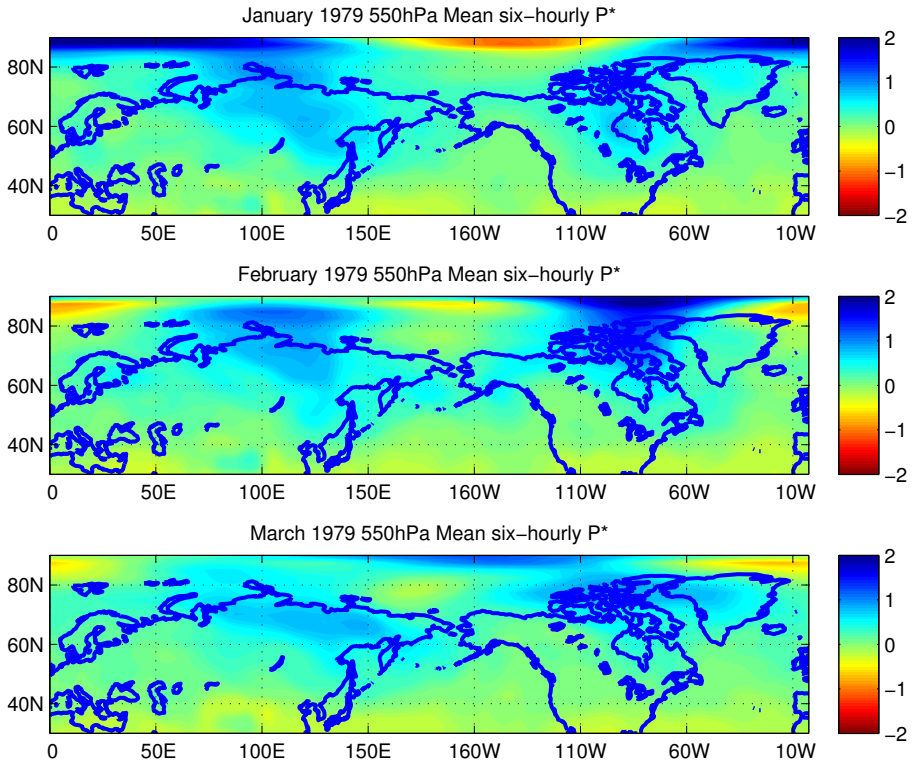

FIGURE A. 47. NCEP - 550 hPa P* from January, February, and March 1979 in PVU

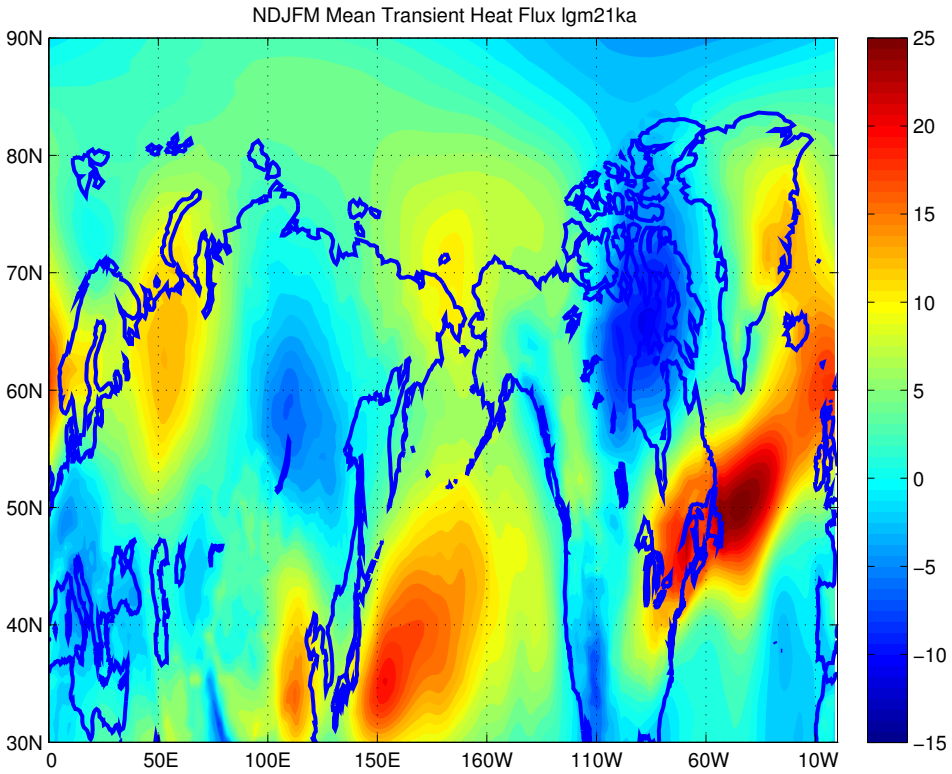

FIGURE A. 48. November through March mean transient eddy heat flux during the last glacial maximum in K*m/s

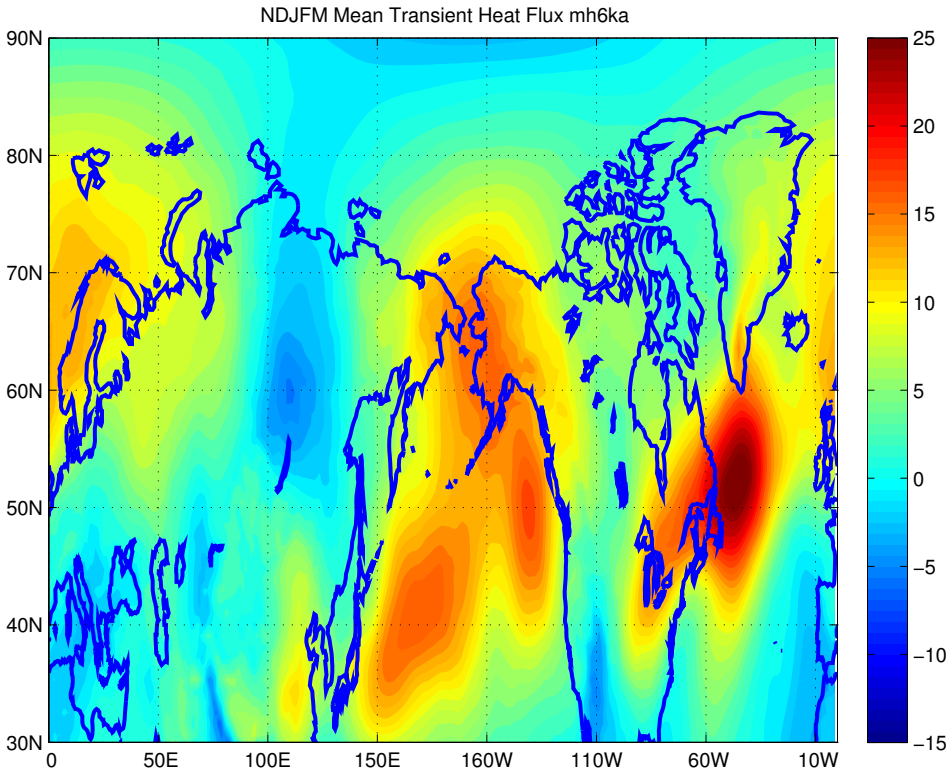

FIGURE A. 49. November through March mean transient eddy heat flux during the mid-Holocene in K*m/s

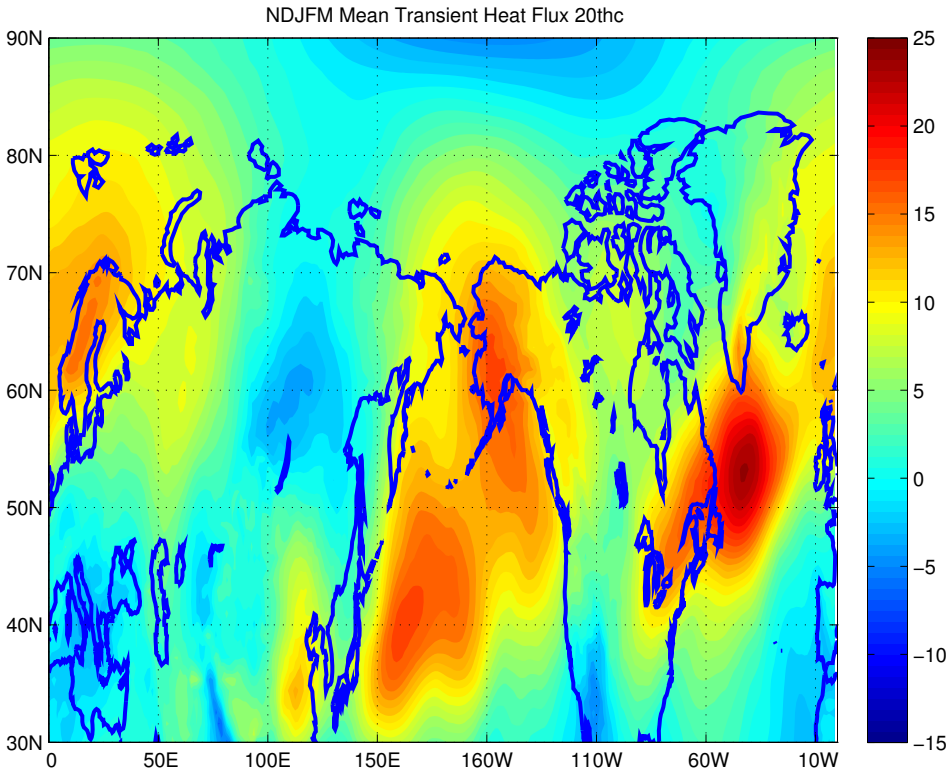

FIGURE A. 50. November through March mean transient eddy heat flux during the 20th century in K*m/s

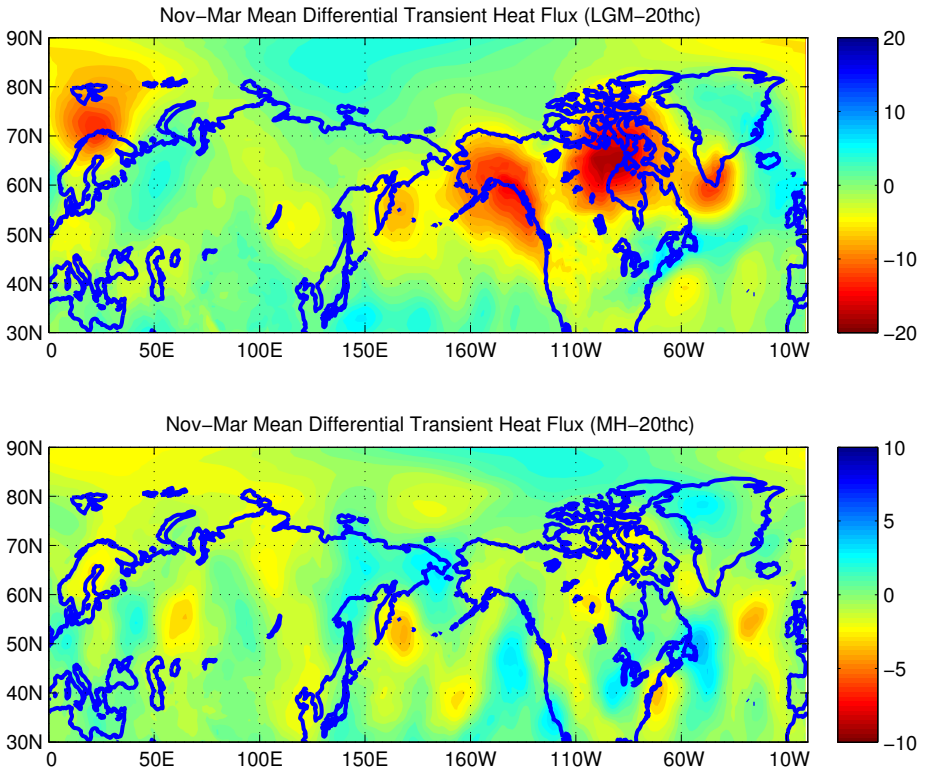

FIGURE A. 51. November through March differential mean transient eddy heat flux between the last glacial maximum and the 20th century (top) and the mid-Holocene and the 20th century (bottom) in K*m/s. Note the difference in scale.

APPENDIX B

TABLES

TABLE B. 1. Normalized Sea Ice Fraction

Era:	LGM	MH	20thc
Jan	0.8312	0.7553	0.7201
Feb	0.8251	0.7636	0.7353
Mar	0.8166	0.7638	0.7332
Apr	0.8050	0.7522	0.7164
May	0.7779	0.7053	0.6614
Jun	0.7316	0.6203	0.5744
Jul	0.6819	0.5044	0.4648
Aug	0.6519	0.3837	0.3549
Sep	0.6788	0.3814	0.3496
Oct	0.7486	0.5141	0.4675
Nov	0.8090	0.6326	0.5860
Dec	0.8303	0.7206	0.6761

TABLE B. 2. Total Transient Eddy Heat Flux (J kg^{-1} m/s)

Era:	LGM-20thc	MH-20th
NH	-2.8534x10^7	-3.1476x10^6
Arctic	-1.8866x10^7	-2.6216x10^6